Quaternary Science Reviews 183 (2018) 140–156

Contents lists available at ScienceDirect

Quaternary Science Reviews

journal homepage: www.elsevier.com/locate/quascirev

Quaternary glaciation of the Lato Massif, Zanskar Range of the NW Himalaya

Elizabeth N. Orr [a, *], Lewis A. Owen [a], Sourav Saha [a], Marc W. Caffee [b, c], Madhav K. Murari [d]

[a] Department of Geology, University of Cincinnati, Cincinnati, OH 45221, USA
[b] Department of Physics, Purdue University, West Lafayette, IN 47907, USA
[c] Department of Earth, Atmospheric and Planetary Sciences, Purdue University, West Lafayette, IN 47907, USA
[d] Department of Geography, Justus Liebig University Giessen, Giessen, Hessen 35390, Germany

ARTICLE INFO

Article history:
Received 6 September 2017
Received in revised form
5 January 2018
Accepted 9 January 2018
Available online 6 February 2018

Keywords:
Zanskar Range
Glaciation style
Cosmogenic isotopes
ELA
Till deposits

ABSTRACT

The glacial chronostratigraphy and history of the Lato Massif of Zanskar northern India is defined for the first time using geomorphic mapping and ^{10}Be surface exposure dating. Three local glacial stages, the Lato, Shiyul and Kyambu, are dated to 244–49, 25–15 and 3.4–0.2 ka, respectively. The Lato glacial stage was the most extensive period of glaciation, characterized by expanded ice caps with glaciers advancing to ~16 km from their present position. Large till deposits are associated with this glacial stage, which represent a time of heightened glacial erosion and localized incision, and increased rates of sediment transfer and deposition. The glacial style transitioned to entrenched valley glaciation during the Shiyul glacial stage. Hummocky moraine complexes reflecting fluctuating glacier margins characterize this glaciation. Glaciers have been confined to the cirques and headwalls of the massif during and since the Kyambu glacial stage. Equilibrium-line altitude (ELA) reconstructions help define the shifts in glaciation over time, with ELA depressions changing from 470 ± 140, 270 ± 80 to 100 ± 30 m for the Lato, Shiyul and Kyambu glacial stages, respectively. The change of glacial style during the latter part of the Quaternary is similar to other regions of the Transhimalaya and Tibet suggesting that this pattern of glaciation may reflect regional climatic forcing. The evolution of the Lato Massif from an isolated alpine plateau to a steeply incised massif over the last several glacial-interglacial cycles may have also influenced the shifts from ice cap to valley glaciation.

1. Introduction

Much attention has been paid to defining the extent and timing of glaciation throughout the Himalayan-Tibetan orogen over the past few decades (Owen and Dortch, 2014 and references therein). This has been mainly motivated by the desire to examine the relative roles of the Asian summer monsoon and mid-latitude westerlies in driving glaciation (Benn and Owen, 1998; Seong et al., 2007; Bookhagen and Burbank, 2010; Bolch et al., 2012; Sharma et al., 2016). These two dominant climatic systems create strong east-west and north-south precipitation gradients across the 2400-km-length and 300-km-breadth of the mountain belt, respectively (Burbank et al., 2003; Owen and Dortch, 2014). The southern and eastern extents of the mountain belt undergo enhanced summer precipitation by the advection of moisture from the Indian Ocean by the Asian summer monsoon (Benn and Owen, 1998; Owen, 2009). The mid-latitude westerlies bring maximum winter precipitation to the western end of the Himalaya from the Mediterranean, Black and Caspian seas (Benn and Owen, 1998; Owen, 2009). These climatic systems and the precipitation gradients they produce have varied significantly throughout the Quaternary as a result of changes in insolation (Finkel et al., 2003; Bookhagen et al., 2005; Owen et al., 2008). This, and microclimatic variations, are considered to have a strong influence upon the nature and timing of glaciation throughout the orogen, and likely responsible for the asynchronous behavior glaciation observed between individual mountain ranges (Benn and Owen, 1998; Bookhagen and Burbank, 2010; Dortch et al., 2011; Owen and

* Corresponding author.
E-mail addresses: orreh@mail.uc.edu (E.N. Orr), owenls@ucmail.uc.edu (L.A. Owen), sahasv@mail.uc.edu (S. Saha), mcaffee@purdue.edu (M.W. Caffee), madhav.murari@geogr.uni-giessen.de (M.K. Murari).

https://doi.org/10.1016/j.quascirev.2018.01.005
0277-3791/

Dortch, 2014).

Through the application of field mapping, remote sensing and numerical dating methods, modern glacial geologic studies across the Himalaya and Tibet provide evidence of significant glacier advances within the last several glacial cycles, with many valleys preserving confirmation for at least four of these advances during the late Quaternary (Owen and Dortch, 2014). Complex variations in the timing and extent of late Quaternary glaciation have been recognized over relatively short distances (10^{1-2} km). This is illustrated well at the western end of the Himalayan-Tibetan orogen, where the local last glacial maximum (lLGM) occurred at different times with vastly different glacier extents (Hedrick et al., 2011; Owen and Dortch, 2014). Within semi-arid regions of the Transhimalaya and Tibet, the style of glaciation has changed significantly over the last several glacial cycles, from expanded ice caps to entrenched valley glaciation (Seong et al., 2009a; Owen et al., 2010; Owen and Dortch, 2014). Rather than a single driver of Himalayan glaciation and its associated landscape change, the timing and extent of glaciation and the preservation of glacial evidence is likely governed by a complex combination of different factors specific to each locality, including climate and microclimate regimes, topographic controls and geologic setting (Bhutiyani, 1999; Hobley et al., 2010; Dortch et al., 2011; Dietsch et al., 2015).

Defining the changes in style and timing of glaciation throughout the Himalayan-Tibetan orogen is an essential component for understanding of the forcing factors behind glaciation and the associated landscape and paleoenvironmental change (Molnar and England, 1990; Brozovic et al., 1997; Barnard et al., 2004, 2006; Korup and Montgomery, 2008; Bookhagen and Burbank, 2010; Ali et al., 2013). The development of robust glacial chronostratigraphies is a prerequisite for examining the complex Quaternary glacial history of the Himalayan-Tibetan orogen. With this in mind, we examine an area of the Lato Massif, an unstudied region of Zanskar in northern India, at the climatic transition between the monsoon influenced Lahaul Himalaya and the semi-arid continental interior of the Transhimalaya (Hedrick et al., 2011). The Lato Massif is an interesting topographic high, which may have influenced the glaciation style over time from a small ice cap to cirque glaciers. Moreover, the Lato Massif is adjacent to several well-studied areas in northern Zanskar and Ladakh where key glacial chronostratigraphies have been developed (Owen et al., 2006; Hedrick et al., 2011; Sharma et al., 2016; Orr et al., 2017). The primary aim of this study is to examine the nature and timing of the late Pleistocene-Holocene glaciation of the Lato Massif. We develop the first glacial chronostratigraphy for this area using remote sensing, field mapping, geomorphic and sedimentological techniques, equilibrium-line altitudes (ELAs) and ^{10}Be surface exposure dating. We compare our glacial chronostratigraphy with studies from the adjacent regions to discuss possible controls upon the extent, style and timing of Quaternary glaciation for this region of the NW Himalaya.

2. Regional setting

The Lato Massif is located in the north-central region of Zanskar. Bounded by the Ladakh Range to the north and the High Himalaya to the south, the Zanskar Range is a semi-arid mountain range within the Transhimalaya of northern India. Zanskar is characterized by discrete west-northwest trending mountain ranges that rise from elevations of ~3500 m above sea level (asl) within the Indus River valley to peaks in excess of 6000 m asl. However, the trend of the Lato Massif which is part of the Mata nappe, is oblique to Zanskar's main ranges, trending northwest and rising from ~4000 to 6150 m asl (Fig. 1).

The formation and development of the Zanskar Range is the result of the on-going continental collision and partial subduction between the Indian and Eurasian lithospheric plates that commenced at ~55 Ma (Schlup et al., 2003). This large-scale tectonism secured the closure of the Neo-Tethys Ocean and the establishment of major geologic structures including the Indus-Tsangpo Suture Zone (ITSZ) and the Zanskar Suture Zone (ZSZ) (Steck et al., 1998, Fig. 1A). The lithotectonic units of the Tethyan Himalaya, Tso Moriri Nappe and North Himalayan crystalline sequence characterize the Zanskar Range. The Lato Massif is a core complex composed of granite and orthogneiss, surrounded by late Cenozoic-Precambrian metasedimentary rocks (Searle, 1986; Steck et al., 1998; Schlup et al., 2003).

Geomorphic studies have described a broad range of valley types in Zanskar, which include steep relief valleys with narrow valley floors and fluvial gorges, to broad and gently sloping valleys with wide cultivated floors (Osmaston, 1994). These valleys have been shown to retain evidence of glacial, fluvial, paraglacial and periglacial landforms and deposits, which include moraines, mass movements, debris flow/alluvial fans and cones, terraces, and outwash and till deposits (Mitchell et al., 1999; Taylor and Mitchell, 2000; Sharma et al., 2016; Orr et al., 2017). Many studies have focused on investigating the past and present glaciation of the mountain range enabled by the excellent preservation of geomorphic evidence (*ibid*). Moreover, with parts of Zanskar remaining unglaciated during the late Quaternary, the Zanskar Range has become a desirable location to understand the role and interplay of geomorphic processes including fluvial and glacial erosion, within semi-arid landscapes (Osmaston, 1994; Hedrick et al., 2011; Jonell et al., 2018).

Climatic and weather records from Leh's Meteorological Station are considered representative of Zanskar's semi-arid climate (Osmaston, 1994). Approximately 40% of the 113 mm a^{-1} of precipitation that falls in Leh occurs between July and September (Osmaston, 1994; Damm, 2006). The Tropical Rainfall Measuring Mission (TRMM) 12-year mean total annual rainfall data shows that Zanskar's mean annual rainfall is < 100 mm (Bookhagen and Burbank, 2006, 2010). Based upon the proposed environmental lapse rate of Derbyshire et al. (1991; ~1 °C/170 m), at the elevations of the contemporary glaciers in Zanskar (5500–6150 m asl), the summer (-7– -1 °C) and winter (−16– -10 °C) temperatures are likely to be significantly lower than in Leh at ~3300 m asl (January [-2.8–14 °C], June [10.2–24.7 °C]).

The desert steppe vegetation and sandy-gravel soils of Zanskar are mostly restricted to elevations below 5000 m asl. Alpine desert vegetation including small leafed shrubs and grasses are present, or no vegetation exists at all, at higher elevations (Osmaston, 1994).

Glacial studies of the Zanskar and Ladakh region have recognized evidence for three to four glacier advances within most investigated valleys, many of these advances occurring during the last few glacial cycles (Owen et al., 2006; Dortch et al., 2010; Hedrick et al., 2011; Lee et al., 2014; Sharma et al., 2016; Orr et al., 2017). Low erosion rates (at the lower end of 0.7–127 m/Ma determined by Dietsch et al., 2015) in parts of this region allow moraines to be preserved for many thousands of years in some valleys (Owen et al., 2010). Through numerical dating methods and existing nomenclature, the glacier advances are commonly assigned to: the lLGM, the global last glacial maximum (LGM as ~ 26–19 ka in MIS 2 as defined by Clark et al., 2009), the late glacial, the neoglacial and the little ice age (LIA) (Owen, 2009; Owen and Dortch, 2014). Orr et al. (2017) provides a summary of the glacial studies for the Zanskar Range. Of particular relevance is the glacial chronostratigraphy for southeast Zanskar produced by Hedrick et al. (2011) who identified four glacial stages extending to >300 ka. Four glacial stages were also defined within the Stok valley of northern Zanskar dating back to 124 ka (Orr et al., 2017).

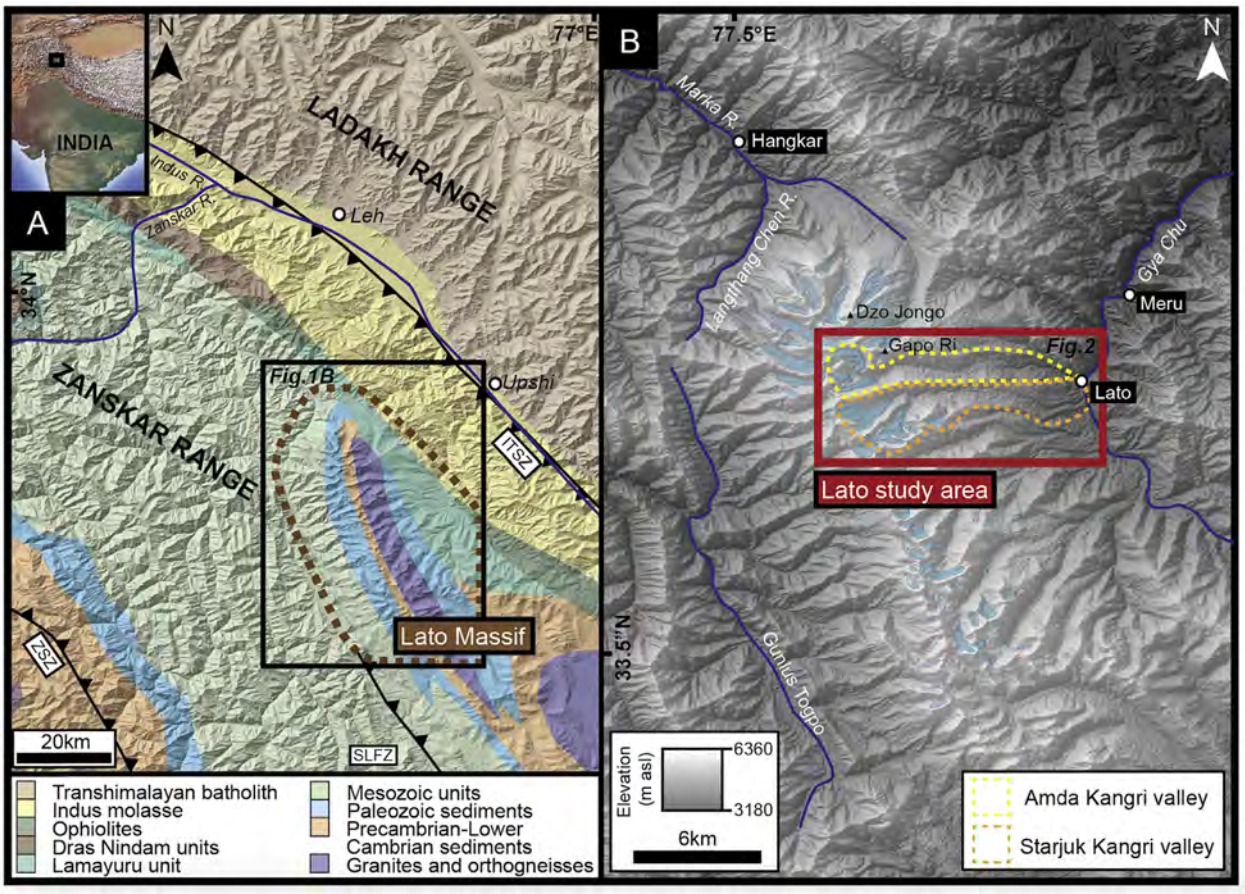

Fig. 1. (A) Location of the Lato Massif study area (outlined by the dashed brown polygon) overlying a simplified digital elevation model and geology map of the Ladakh region, northern India (modified from Schlup et al., 2003). (ITSZ - Indus-Tsangpo Suture Zone; ZSZ - Zanskar Suture Zone, SLFZ - Sarchu-Lachung La Fault Zone). Inset map illustrates the location of the Ladakh region within the Himalayan-Tibetan orogen (base map from geomapapp.org). (B) Location of the Lato study areas (outlined by red box) superimposed over an ASTER digital elevation model of the Lato Massif (in part A). The light blue polygons show the positions of contemporary glaciers. (For interpretation of the references to colour in this figure legend, the reader is referred to the Web version of this article.)

Nagar et al. (2013) and Sharma et al. (2016) have suggested that in this region, glaciers respond to small fluctuations in precipitation governed by the mid-latitude westerlies.

Using ^{10}Be dating of Ladakh Range moraines and a synthesis of previous studies, Dortch et al. (2013) developed a regional glacial chronostratigraphy, in which they defined the semi-arid western Himalayan-Tibetan glacial stages (SWHTS). Dortch et al. (2013) proposed that SWHTS stages older than 21 ka are broadly correlated with strong monsoons, while those stages that are 21 ka or younger, broadly correlate with global ice volume and northern hemisphere climatic events such as the Oldest Dryas, Older Dryas, Younger Dryas, Roman Humid Period, and LIA.

3. Methodology

3.1. Field methods

Amda Kangri (kangri meaning glacier) and Starjuk Kangri valleys were examined in detail on the eastern side of the Lato Massif (Fig. 1B). These valleys were chosen because they are presently glaciated with small glaciers (~1–10 km^2), have an abundance of well-preserved landforms and thick successions of Quaternary sediment, and because these valleys are readily accessible for fieldwork.

Detailed geomorphic maps were constructed in the field, aided by Landsat ETM + data, Google Earth Imagery and a three arc-second (~90 m) Shuttle Radar Topography Mission (SRTM) digital elevation model (DEM). The location of landforms and ^{10}Be samples was recorded using a handheld Garmin Etrex 30 GPS unit. Remote sensing and field-based geomorphic and sedimentological analysis was used to differentiate between landforms and sediment deposits using the methods described in Benn and Owen (2002).

Moraines within the Amda Kangri and Starjuk Kangri valleys were divided into three groups, each representing a local glacial stage using the morphostratigraphic methods advocated by Hughes et al. (2005) and Hughes (2010) (Table 1). From oldest to youngest, we call these the Lato, Shiyul, and Kyambu glacial stages. The best-preserved well-defined moraine crests for each of the glacial stages were selected for further investigation and ^{10}Be dating. In total, nine moraines were selected, four from the Lato, two from the Shiyul, and three from the Kyambu glacial stages. The Amda Kangri valley had the best-preserved moraines, and therefore only two moraines were sampled in the Starjuk Kangri valley. Moraines were numbered from youngest to oldest (*1* to *n*) and a subscript was assigned for the studied valley and moraine (*AK* = Amda Kangri valley; *SK* = Starjuk Kangri valley). The moraine M_{AK1} for example, is the youngest moraine (subscript 1) of the Amda Kangri valley (subscript *AK*), located closest to the contemporary glacier. M_{AK7} is located furthest downstream from the glacier with the greatest amount of weathering evident, representing the oldest and maximum extent of glaciation within the valley. Each moraine is considered representative of a glacial advance/substage within a

Table 1
Descriptions of the local glacial stages of the Lato study area.

Glacial stages	Moraine	Moraine characteristics	Boulder characteristics
Lato	M_{AK5} M_{SK2} M_{AK6} M_{AK7}	- Single, high-moderately denuded yet stable lateral and latero-frontal moraines. - Pebbly diamicton with a sandy-gravel matrix. - Some xerophytic shrubs and grasses, and soil development	- Subangular/subrounded boulders distributed along the crests of the moraine ridges. - Stable and well-set boulders. - High-moderately weathered (cavernous weathering, evidence of varnish and exfoliation).
Shiyul	M_{AK4} M_{SK1}	- Stable, latero-frontal moraines from hummocky moraine complexes. - Moderately weathered pebbly diamicton with a sandy-gravel matrix. - Some xerophytic shrubs and grasses, and soil development.	- Subangular/subrounded boulders distributed along the crests of the moraine ridges. - Stable and well-set boulders. - Moderate weathering (some pitting and exfoliation).
Kyambu	M_{AK1} M_{AK2} M_{AK3}	- Unstable, slightly weathered, and sharply crested terminal moraines (part of a moraine complex). - Diamicton of boulders and cobbles (clast-supported) with coarse gravel matrix. - No vegetation or soil development	- Angular/subangular boulders covering the entirety of landforms. - Combination of well and poorly set boulders. - Slight weathering (minor exfoliation). - Some evidence of frost action.

local glacial stage. Assigning each moraine to an individual glacial stage was not considered appropriate for this study as several of the moraines shared very similar characteristics, which in addition to the morphostratigraphy of the valleys, suggest three phases of glaciation. These glacial substages are equivalent to the local glacial stages identified throughout the Himalayan-Tibetan orogen such as those described in Owen and Dortch (2014).

We preferentially selected large unweathered or less weathered granitic boulders that were well inset into the moraine crests for ^{10}Be dating. The ^{10}Be concentrations in these types of boulder are most likely to represent the true age of the moraines (Owen, 2009; Heyman et al., 2011; Heyman, 2014).

Approximately 500 g of rock was removed to a depth of 1–5 cm from the upper surface of each boulder using a hammer and chisel, avoiding any areas of obvious weathering and/or exfoliation. Detailed descriptions of each sampled boulder were taken, including location, lithology, morphology, size, weathering, emplacement and topographic shielding (Tables 1 and 2), and the boulders were photographed (Supplementary Item 1). Topographic shielding was measured using an inclinometer, measuring the angle from the boulder surface to the horizon at 10° increments. Multiple boulder samples were collected from each moraine to help address problems associated with prior exposure of boulders to cosmic rays and weathering, exhumation, moraine degradation, boulder toppling and shielding due to snow and/or sediment (Benn and Owen, 2002; Heyman et al., 2011). A combination of these geologic factors can lead to a large spread of ages for a single moraine, including both under- and overestimates of the true age of the moraine (Owen, 2009; Heyman et al., 2011). The ^{10}Be age of each moraine is based on the distribution of boulder exposure ages and provides an estimate for the minimum timing of moraine formation, prior to the glacier beginning to thin or retreat (Ivy-Ochs et al., 2007; Putkonen et al., 2008). Multiple samples from each moraine will help to identify the erroneously young and old ages.

To further define the timing and extent of glaciation during the Kyambu glacial stage, additional bedrock samples were taken for ^{10}Be analysis within the upper extent of the Amda Kangri valley, collectively referred to as B_{AK1} (B = boulder samples; AK = Amda Kangri).

Contemporary glaciers (G) were numbered using a similar approach, a subscript assigned to the valley (AK, SK) and the glacier number (*1–3*). As an example, the Amda Kangri glacier, the largest within the valley is referred to as G_{AK1}.

Tills within the study areas have also been numbered from highest elevations and youngest, to lowest elevation and oldest. Diamicts are numbered from D_1 (youngest) to D_4 (oldest). D_4 is the furthest downstream and with the greatest evidence of weathering.

3.2. ^{10}Be dating methods

Samples for ^{10}Be dating were prepared at the Geochronology Laboratories at the University of Cincinnati following the methods outlined in Dortch et al. (2009) and Orr et al. (2017). AMS measurements were undertaken at the Purdue Rare Isotope Measurement Laboratory (PRIME) at Purdue University (Sharma et al., 2000).

The ^{10}Be surface exposure ages were calculated using the CRONUScale (Marrero et al., 2016), Cosmic Ray Exposure program (CREp; Martin et al., 2017) and CRONUS-Earth V3 online calculators using the Lifton et al. (2014) scaling scheme. Unlike previous schemes, Lifton et al. (2014) accounts for nuclide-specific production rate sensitivities to temporal and spatial variability in geomagnetic and solar inputs. Be-10 ages were also calculated using the other available scaling schemes and production rate models to facilitate future comparisons with other studies (Supplementary Item 2). We assume zero erosion when calculating the ^{10}Be ages because we are unable to define the erosion rates for individual boulders, and the boulders that were sampled exhibited little, if any, evidence of erosion. Moreover, several studies have shown that erosion rates within this region are extremely low (lower end of 0.7–127 m/Ma determined by Dietsch et al., 2015). If we assume an erosion rate of 2.3 m/Ma for the Lato study area, 0–10 ka ages would be underestimated by <10%, a 20 ka age by ~4% and a 100 ka age by ~28% (Seong et al., 2007, 2009b; Owen et al., 2012).

We considered the distribution of boulder ages on each individual moraine to help establish the timing of moraine formation. Outlier ^{10}Be ages for individual boulder/s on a moraine were identified using Chauvenet's criterion, a method that determines the acceptable scatter around the mean value of a population at a 95% confidence interval (Taylor, 1997; Putnam et al., 2013; Supplementary Item 3). The arithmetic mean (simple mean) age for each moraine was calculated alongside a corrected arithmetic mean where the identified outliers were excluded from analysis. We also report the weighted mean age for each moraine, which accounts for the statistical distribution of the exposure ages (Barrows, 2007). For each of these methods, the resultant ages for the arithmetic and weighted methods fall within the uncertainty of one another for each of the nine moraines. The corrected arithmetic mean ages are considered the most representative of the ages for the moraines, as they reflect reasonable minimum age estimates; we refer to them in the remainder of the text. For moraines with only two assigned ages, the corrected weighted mean is used. Each moraine age is considered to be representative of the timing of a

Table 2
Sample details and ^{10}Be ages (uncertainty is expressed as 1σ) for the moraines and bedrock of the Lato study area.

Sample name	Moraine	Glacial stage[a]	M type[b]	Location		Altitude	Boulder size			Lithology[c]	Weathering[d]	Sample thickness	Topographic shielding factor	^{10}Be	Minimum exposure age[e,f]
				Lat (°N)	Long (°E)	(m asl)	Length (m)	Width (m)	Height (m)			(cm)		(10^6 atoms/g)	(ka)
Amda Kangri valley															
LATO-1416*	M_{AK1}	K	T	33.6822	77.5921	5358	5.9	2.9	1.1	Granite	MW/MB	4	0.95	0.02 ± 0.002	0.2 ± 0.03
LATO-1417*	M_{AK1}	K	T	33.6826	77.5920	5348	1.85	1.4	1	Granite	MW/SB	2	0.95	0.03 ± 0.001	0.4 ± 0.03
LATO-1418*	M_{AK1}	K	T	33.6826	77.5921	5351	0.9	0.7	0.7	Granite	MW/SB	3	0.95	0.02 ± 0.001	0.2 ± 0.03
LATO-1419*[1]	M_{AK1}	K	T	33.6827	77.5920	5339	1.1	0.8	0.4	P. granite	MW/MB	3	0.95	0.3 ± 0.02	3.4 ± 0.3
LATO-1409*[1]	M_{AK2}	K	T	33.6851	77.5953	5314	1.8	1.5	0.6	P. granite	SW/SB	3	0.96	2.7 ± 0.06	27.6 ± 1.5
LATO-1410*	M_{AK2}	K	T	33.6851	77.5953	5321	1.8	1.1	0.5	Granite	SW/SB	2.5	0.96	0.2 ± 0.009	3.0 ± 0.2
LATO-1411*	M_{AK2}	K	T	33.6851	77.5952	5315	2.5	1.6	0.9	P. granite	MW/MB	2	0.96	0.3 ± 0.02	4.1 ± 0.3
LATO-1412*	M_{AK2}	K	T	33.6850	77.5957	5315	2.1	0.8	0.7	Granite	MW/MB	1	0.96	0.03 ± 0.002	0.4 ± 0.03
LATO-1413*	M_{AK2}	K	T	33.6849	77.5957	5317	1.7	0.9	0.6	Granite	SW/MB	2	0.96	0.06 ± 0.002	0.7 ± 0.1
LATO-1414*	M_{AK2}	K	T	33.6851	77.5954	5314	2	1.3	1	Granite	SW/DB	2	0.96	0.04 ± 0.002	0.5 ± 0.03
LATO-1415*	M_{AK2}	K	T	33.6822	77.5920	5366	2	1.3	0.9	Granite	MW/MB	3	0.95	0.1 ± 0.003	1.8 ± 0.1
LATO1405	M_{AK3}	K	T	33.6805	77.6211	5134	1.5	1.3	0.5	M. granite	SW/MB	2	0.97	0.1 ± 0.09	2.2 ± 1.4
LATO1408	M_{AK3}	K	T	33.6907	77.6211	5136	1.2	0.9	0.5	Granite	SW/MB	1	0.97	0.1 ± 0.02	1.6 ± 0.3
LATO1426	M_{AK4}	S	LF	33.6911	77.6635	4913	3.4	1.8	1.2	Granite	SW/DB	2.5	0.94	0.9 ± 0.02	15.4 ± 0.4
LATO1427	M_{AK4}	S	LF	33.6903	77.6662	4871	2	1.4	0.9	Granite	SW/SB	2	0.94	0.9 ± 0.03	15.1 ± 0.4
LATO1428[1]	M_{AK4}	S	LF	33.6905	77.6665	4856	1.8	1.4	1.1	Granite	SW/DB	1	0.95	1.4 ± 0.04	21.5 ± 0.7
LATO1429	M_{AK4}	S	LF	33.6730	77.6697	4908	1.9	1.1	0.5	P. granite	SW/SB	5	0.95	1.1 ± 0.02	17.6 ± 0.4
LATO1422	M_{AK5}	L	L	33.6904	77.6537	4939	2.8	2.1	1.1	Granite	MW-HW/DB	1	0.94	3.8 ± 0.06	57.3 ± 1.1
LATO1423	M_{AK5}	L	L	33.6904	77.6540	4939	3.5	2.5	0.9	Granite	MW/DB	3	0.94	3.3 ± 0.06	49.0 ± 1.8
LATO1401	M_{AK6}	L	LF	33.7012	77.6710	4980	1	0.8	0.6	P. granite	MW/MB	2	0.95	7.7 ± 0.1	113.3 ± 2.0
LATO1402	M_{AK6}	L	LF	33.7017	77.6678	5005	2.1	1.7	0.6	P. granite	MW/MB	3	0.95	4.7 ± 0.2	69.9 ± 2.9
LATO1403[1]	M_{AK6}	L	LF	33.7021	77.6643	5039	2.1	2.1	1.1	P. granite	MW/MB	4	0.95	0.1 ± 0.06	1.1 ± 0.1
ZK51	M_{AK7}	L	LF	34.6780	77.7228	4196	1.75	1	0.8	Granite	MW-HW/MB	2	0.95	11.2 ± 0.1	186.6 ± 3.0
ZK52	M_{AK7}	L	LF	33.6780	77.7228	4196	1.5	1.2	0.4	P. granite	MW-HW/SB	2	0.95	8.8 ± 0.3	151.6 ± 6.4
ZK53[1]	M_{AK7}	L	LF	33.6780	77.7226	4205	2.2	1	1.2	Granite	MW/DB	2	0.95	4.4 ± 0.2	75.2 ± 4.3
ZK54	M_{AK7}	L	LF	33.6780	77.7222	4205	1.25	1	50	Granite	MW-HW/MB	2	0.95	11.4 ± 0.2	243.8 ± 6.0
LATO1420	B_{AK1}	K	B	33.6914	77.6081	5191	–	–	–	Granite	MW	2.5	0.95	1.1 ± 0.03	13.7 ± 0.7
LATO1421	B_{AK1}	K	B	33.6913	77.6083	5180	–	–	–	Granite	MW	3	0.95	1.1 ± 0.02	13.6 ± 0.7
LATO1601	B_{AK1}	K	B	33.6911	77.6086	5171	–	–	–	Granite	MW	2	0.94	1.2 ± 0.02	14.4 ± 0.7
Starjuk Kangri valley															
LATO1432	M_{SK1}	S	L	33.6745	77.6792	4851	2.2	1.1	0.5	Granite	MW/DB	2	0.95	1.1 ± 0.09	17.8 ± 1.3
ZK58	M_{SK1}	S	L	33.6747	77.6792	4869	3.5	1.25	1	P. granite	MW/MB	2	0.95	1.8 ± 0.05	23.5 ± 0.6
ZK59[1]	M_{SK1}	S	L	33.6746	77.6793	4859	2	2	1.1	P. granite	MW/DB	2	0.95	0.5 ± 0.03	7.3 ± 0.4
ZK60	M_{SK1}	S	L	33.6749	77.6793	4862	3	1.25	0.8	Granite	HW/DB	2	0.95	2.0 ± 0.05	25.8 ± 0.7
LATO1433	M_{SK2}	L	L	33.6754	77.6933	4723	1.3	1.3	0.6	P. granite	MW/DB	2	0.95	5.8 ± 0.2	98.7 ± 2.5
ZK55	M_{SK2}	L	L	33.6753	77.6945	4729	2	2	1.2	P. granite	MW-HW/DB	2	0.95	7.1 ± 0.1	93.6 ± 2.0
ZK56[1]	M_{SK2}	L	L	33.6752	77.6949	4729	1.75	0.75	0.75	Gneiss	MW-HW/DB	2	0.95	4.6 ± 0.4	58.8 ± 5.7
ZK57	M_{SK2}	L	L	33.6749	77.6949	4719	1.25	1	0.5	P. granite	MW/MB	2	0.95	6.5 ± 0.3	85.3 ± 3.9

*Dataset first presented by Saha et al. (2018).
[1]Sample ages identified as outliers.
[a] Glacial stage: K- Kyambu, S- Shiyul, L- Lato.
[b] Moraine type: L-lateral, LF- latero-frontal, T-terminal. B- bedrock.
[c] P. granite-porphyritic granite, M. granite-metagranite
[d] Boulder weathering characteristics: SW- slightly weathered (no pitting), MW- moderately weathered (some pitting, moderate exfoliation), HW- Highly weathered (exfoliated sheets can be manually pulled off the rock), SB- slightly buried, MB- moderately buried, DB- deeply buried.
[e] Production rate for the CRONUS and CREP calculator is $5.10 \pm 0.26 \times 10^{-7}$ ^{10}Be atoms/grams SiO_2/year and a ^{10}Be half-life of 1.36Ma.
[f] Minimum exposure age is calculated using the Balco et al. (2008) calibration dataset and Lifton et al. (2014) calculation scheme.

local glacial substage for the Lato study areas. The timing and duration of the local glacial stages (Lato, Shiyul and Kyambu) are broadly defined by the collective age range (oldest to youngest) of the relevant glacial substages within the Lato Massif. The identified outliers of the Lato chronology are not used to define the timing of its glacial stages. Consistent with other glacial studies, additional statistical analysis such as probability density functions was considered unnecessary and ambiguous for the Lato record due to the relatively small dataset size, where some moraines are dated with only two ages (Owen et al., 2012; Orr et al., 2017).

Thirty-seven new ^{10}Be ages are used to construct the glacial chronostratigraphy for the Lato Massif. The 11 ages that define the Kyambu glacial stage are also presented in Saha et al. (2018) that provides an evaluation of the timing of Holocene glaciations throughout the western end of the Himalayan-Tibetan orogen.

3.3. ELA reconstructions

Past and present equilibrium-line altitudes (ELA) and ELA depressions (ΔELA) were calculated using the methods highlighted in Osmaston (2005), Heyman (2014), Sharma et al. (2016), and Orr et al. (2017). These include area-altitude (AA), area accumulation ratios (AAR) and toe-headwall accumulation ratios (THAR). Ratios of 0.4, 0.5 and 0.6 were used for the AAR, and 0.4 and 0.5 for the THAR methods, as in other studies throughout the NW Himalaya (Seong et al., 2008; Dortch et al., 2010; Orr et al., 2017). The mean of the AA, AAR and THAR values were used to estimate the ELAs for the contemporary and former ice extents in our study, to help reduce the uncertainties associated with any one of these methods (Benn et al., 2005).

4. Landforms descriptions

The Lato Massif stretches for ~40 km, some 40 km southwest of the ITSZ and ~160 km northeast of the ZSZ (Fig. 1A and B). A steep arête forms a drainage divide between the north, northeast and southwest facing glaciated and unglaciated valleys of the Lato Massif. The arête has high altitude peaks (>6000 m asl) and steep relief headwalls in our study area and in the wider massif. Streams mainly drain northeast or southwest into the Zanskar or Markha rivers, respectively. These rivers ultimately drain into the Indus River.

4.1. Amda Kangri study area

The Amda Kangri study area is a ~17-km-long northwest trending valley on the northeast flank of the Lato Massif (Figs. 1B and 2). Three contemporary glaciers occupy the upper ~2.5 km of the study area ($G_{AK1\text{-}3}$, ~5350–5800 m asl). The upper extent of the valley is narrow with steep (30–70°) bedrock walls, which widen down-valley to gentler (10–20°) hillslopes that support a thick veneer of saprolite, talus and/or till. The Amda Kangri valley becomes a steep-sided gorge ~7 km down-valley from its headwall, where the Amda River has incised through extensive valley fills composed predominantly of till.

A succession of well-preserved moraines extends the full extent of the Amda Kangri valley, including larger multi- and single ridged lateral and terminal moraines, and smaller recessional moraines and hummocky terrain (M_{AK1}–M_{AK7}). These moraines become progressively more weathered down-valley with denuded and subdued forms, and overlying boulders becoming more rounded, with deep pits and evidence of cavernous weathering. Debris cones, alluvial fans, terraces and till and sediment deposits that further characterize the valley, are also more deeply eroded in the lower stretches of the study area.

M_{AK7} is a subdued and high-moderately denuded latero-frontal moraine at the mouth of the Amda Kangri valley. Subangular to

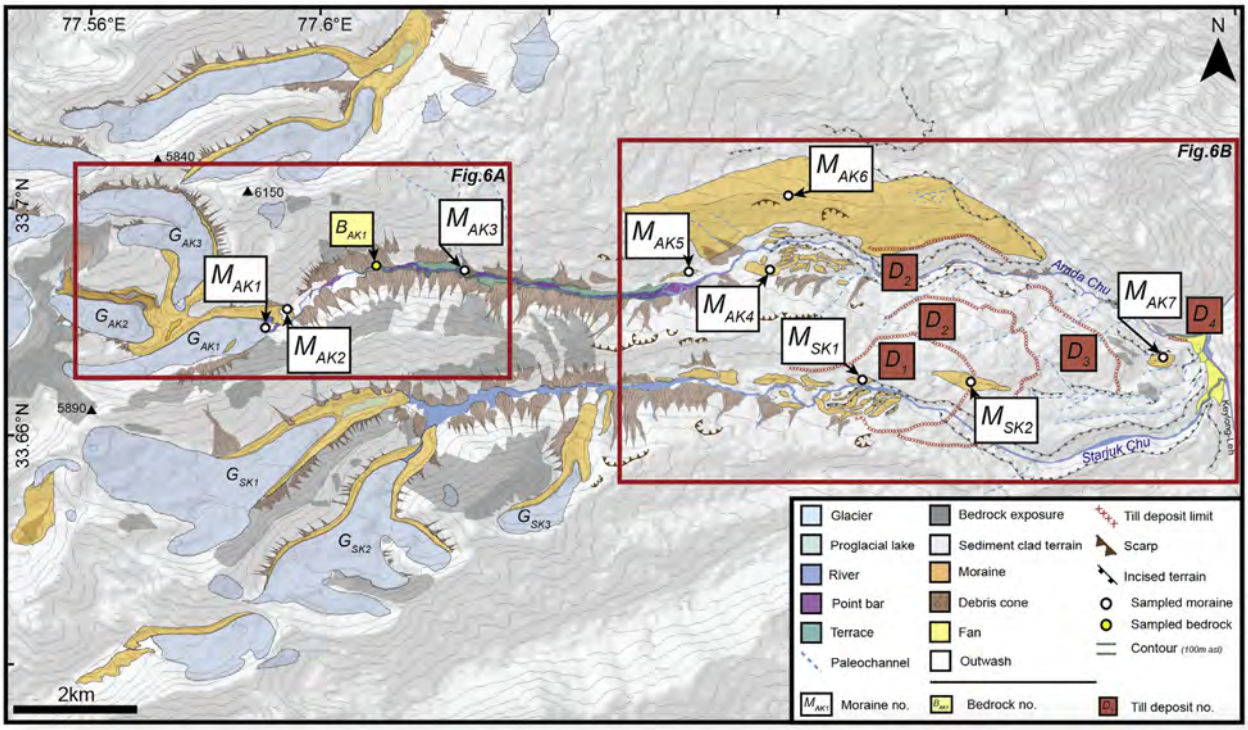

Fig. 2. Geomorphology of the study areas on the east side of the Lato Massif showing the location of the main moraines examined in this study (see Fig. 1B for location of study area). Location of bedrock samples and till deposit limits are also highlighted. Red boxes outline the detailed geomorphic maps shown in Fig. 6. (For interpretation of the references to colour in this figure legend, the reader is referred to the Web version of this article.)

rounded boulders are distributed across the two subtle ridges of this gravelly diamicton. Surface boulders have rock varnish on them with deep pits and cavernous weathering.

M_{AK6} at ~5100 m asl is a single crested latero-frontal moraine, and is composed of a high-moderately weathered matrix-supported gravelly diamicton, and sparsely covered with xerophytic shrubs. This is the largest moraine in the study area and measures ~6 km in length. The margins of the landform are highly incised with surficial evidence of mass movements and gullying. The southern flank of M_{AK6} is overlain by till. Subrounded-subangular boulders are distributed across the full extent of the moraine, the most stable and well-set boulders are present along the subdued crest. The boulders have rock varnish on them and are moderate-highly weathered and exfoliated.

M_{AK5} is a ~500-m-long low-relief lateral moraine positioned on the valley side at ~4900 m asl. The moraine is composed of a high-moderately weathered matrix-supported gravelly diamicton with large well-set tabular boulders across its surface. The surface boulders have rock varnish and exhibit some exfoliation and spallation. M_{AK5} has some sandy-gravel soil development and xerophytic shrubs distributed across the moraine at irregular intervals.

M_{AK4} is a ~750-m-long latero-frontal moraine, and is the least denuded moraine ridge of a hummocky moraine complex at ~4860 m asl, some 1 km west of M_{AK5}. The landform is composed of a moderately weathered pebbly diamicton with a sandy-gravel matrix, supporting some sandy soil development and xerophytic shrubs and grasses. Subangular–rounded surface boulders are sparsely distributed along the crest of the moraine. Minor exfoliation and rock varnish is evident on some of these boulders.

M_{AK3} is a single crested ~150-m-long terminal moraine that trends south, at an altitude of ~5110 m asl. This moraine is composed of a pebbly diamicton with a sandy-gravel matrix, and is covered by a thick veneer of subrounded–angular boulders and frost-shattered debris. The landform is low-moderately weathered, with surface boulders that are slightly exfoliated and cracked.

M_{AK2} is a north trending multi-crested moraine that is part of the moraine complex bordering the snout of Amda Kangri (G_{AK1}) at ~5225 m asl, some 2.5 km upstream from M_{AK3}. The moraine is composed of a clast-supported diamicton of slight-moderately weathered subangular–angular cobbles and boulders within a sandy-gravel matrix. Surface boulders and frost-shattered debris cover the entire surface of the landform, with some of these surface boulders being well inset into the moraine. There is no evidence of landslide/rockfall debris on this moraine despite being close to the steep valley sides.

M_{AK1} is a ~150 m long, steep and sharp-crested terminal moraine at the snout of the G_{AK1}, part of the same moraine complex as M_{AK2}. This moraine shares similar sedimentological and weathering characteristics to M_{AK2}.

The B_{AK1} bedrock (5180 m asl) is located ~1.4 km downstream from M_{AK2}, and exhibits some evidence of glacial polish and striations.

4.2. Starjuk Kangri study area

The Starjuk Kangri study area is a ~17-km-long northwest trending valley, directly south of the Amda Kangri valley (Figs. 1B and 2). In addition to Starjuk Kangri (G_{SK1}), this valley contains two glaciers (G_{SK2} and G_{SK3}), one sourced from the catchment's headwall and the other from a smaller sub-catchment at ~5500 m asl.

The valley morphology changes down-valley in a similar way to the Amda Kangri valley, and contains similar glacial and paraglacial landforms and deposits. Consequently, the successions of moraines that are preserved throughout the full extent of the valley have similar weathering characteristics down-valley as those of the Amda Kangri valley.

M_{SK1} and M_{SK2} in the lower stretches of the valley overlay the extensive till deposits. M_{SK2} is a low-relief moderately weathered lateral moraine that overlies till deposits D_1 and D_2. This ~1-km-long moraine is composed of a matrix-supported gravelly diamicton, and has a single subdued crest with some soil development and vegetation. Well-inset moderate–highly weathered boulders (exfoliation, pitting) are sparsely distributed across the surface of the landform.

M_{SK1} is a single-crested lateral moraine that is part of the hummocky moraine complex overlying the D_1 till deposit at ~4840 m asl, some 1.3 km east of M_{SK2}. This ~300-m-long landform is a moderately weathered pebbly diamicton with well-developed sandy-gravel soils and xerophytic shrubs. Well-inset subangular–rounded boulders with evidence of slight-moderate weathering (exfoliation, spallation) are present across the moraine crest.

4.3. Till deposits in the Amda Kangri and Starjuk Kangri valleys

Four till deposits are present within the lower ~6 km of the Amda Kangri and Starjuk Kangri valleys at altitudes between ~4000 and 4900 m asl (Figs. 2 and 3). The tills become slightly more weathered downstream with greater evidence of fluvial down-cutting by the Amda and Starjuk rivers and paleochannels, gullying and overland erosion. Surface boulders exhibited evidence of rock varnish and cavernous weathering. Natural exposures into the tills are few, but where present they reveal matrix-supported sandy-gravel diamicts with angular to subrounded boulders and cobbles (Fig. 3D; 3E). Unconsolidated, with no deformation structures indicative of subglacial sediment, these tills are likely composed of supraglacial till. The till surfaces and exposures are too degraded for the application of cosmogenic surface exposure dating. Cosmogenic burial age dating was not attempted because of the lack of locations with significant overburden, although isochron burial age dating may be attempted in future studies given appropriate resources. The lack of fine non-glacial sediment in the available exposures inhibited the use of OSL methods for dating these deposits.

The D_4 till deposit underlies M_{AK7} and extends to the mouth of both valleys (~4000 m asl; Fig. 2). This till has been denuded and incised to a greater extent than D_1–D_3. The D_3 till extends to an elevation of ~4620 m asl, some 500 m upstream of M_{AK7}. Streams have deeply incised into this till deposit. D_2 underlies M_{SK2} and overlies M_{AK6} and extends to a minimum elevation of ~4400 m asl within the valleys: the deposit has been incised by the Amda and Starjuk rivers. D_1 extends exclusively from the Starjuk Kangri valley to an elevation of ~4680 m asl. There is no evidence of this deposit in the Amda Kangri valley. D_1 underlies the M_{SK1} hummocky moraine complex and M_{SK2}.

4.4. Assigning local glacial stages

The degree of landform degradation and surface weathering characteristics varies within the Lato Massif; from very fresh and well-preserved moraines, to highly weathered and degraded moraines. These characteristics helped assign the moraines to a particular glacial stage (Table 1, Fig. 4). This means that unlike other glacial studies, several glacial substages or moraines which each represent one or more glacial advances, define each of the Lato Massif local glacial stages. Regional glacial stages are made up of a combination of local stages across a region that statistically have the same ages.

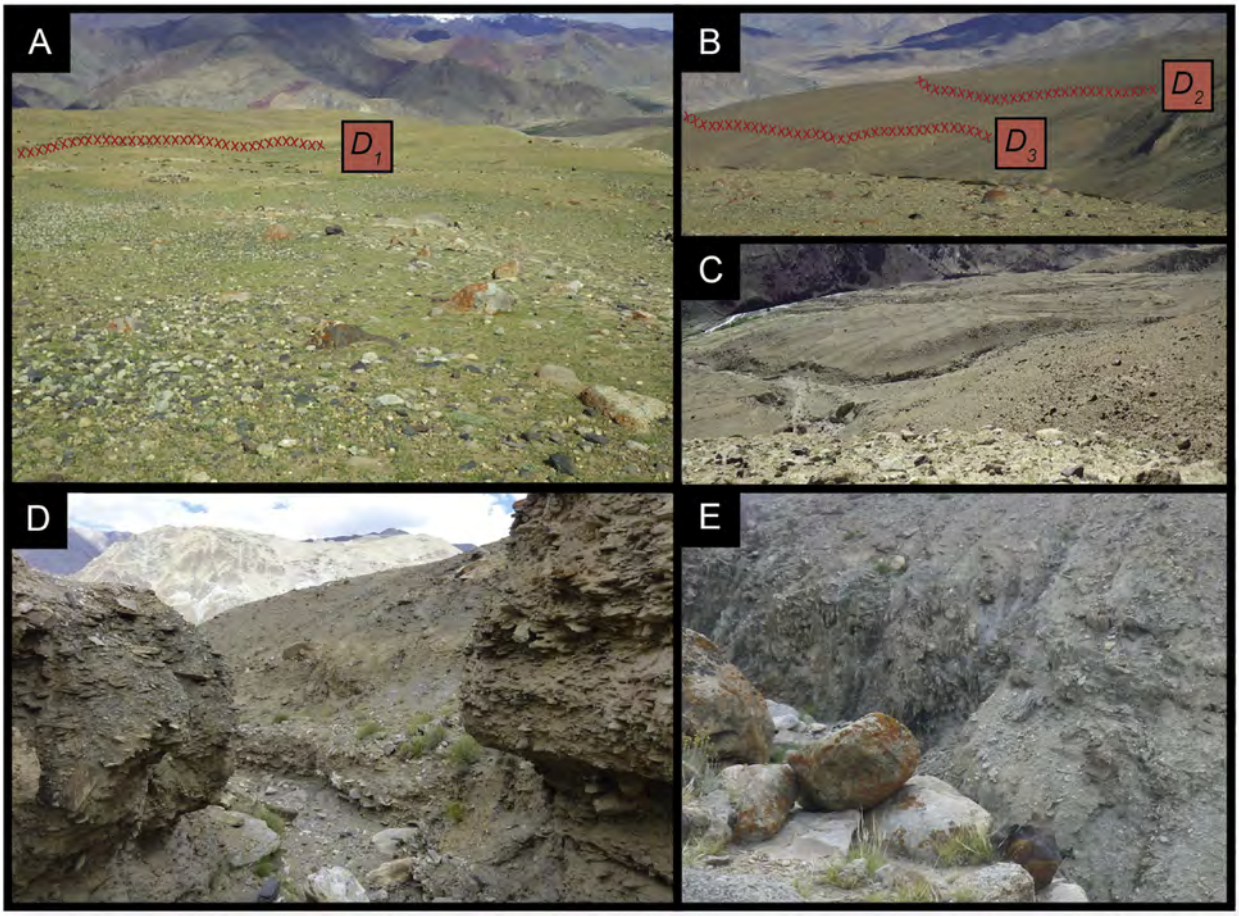

Fig. 3. Views of till deposits in the detailed study areas. (A) Surface of the D_1 till in the Starjuk Kangri valley (red cross lines denote location of till limits herein). (B) M_{AK6} moraine (foreground) and limits of the D_2 and D_3 deposits. (C) D_3 at the mouth of the Starjuk Kangri valley viewed from the M_{AK7} moraine. (D) D_3 till exposures (~5 m high) from within an incised paleochannel. (E) D_4 till deposit incised (gully depth of ~10 m) by paleochannel (background). Boulders in foreground overly alluvial fan sediment at the mouth of the Starjuk Kangri valley. (For interpretation of the references to colour in this figure legend, the reader is referred to the Web version of this article.)

5. ^{10}Be dating

5.1. Amda Kangri study area

The ^{10}Be ages in the Amda Kangri valley are consistent with the morphostratigraphy, in that the ages are progressively older for each morphostratigraphically older moraine (Figs. 5 and 6, Tables 2 and 3). The chronology also confirms that despite M_{AK5} being upstream of M_{AK4}, its position on the hillslope and its geomorphic descriptions show that it records an older glacial substage/advance. M_{AK5} has been preserved within the valley because of its positioning beyond the limits of the following M_{AK4} glacier advance (Fig. 4).

The ^{10}Be boulder exposure ages for M_{AK7} range between 243.8 ± 6 and 75.2 ± 4.2 ka, with a corrected mean age of 194 ± 46.4 ka (uncertainties for all arithmetic means are 1σ).

The ^{10}Be ages for M_{AK6} range from 113.3 ± 2 to 1.1 ± 0.1 ka. Based upon these ages and the morphostratigraphy of the valley, the 1.1 ± 0.1 ka age (LATO1403) is considered an outlier. This very young exposure age could be the result of the weathering identified on this boulder's surface and/or the observed high-moderate degradation of the moraine. After eliminating LATO1403, the chronology of M_{AK6} is now defined by only two ^{10}Be ages; its age accordingly less robust. The corrected weighted mean age of this moraine is therefore 99.4 ± 1.4 ka.

The two ages for M_{AK5} are 57.3 ± 1.1 and 49 ± 1.8 ka, resulting in a weighted mean landform age of 55.2 ± 0.9 ka. Although the age is stratigraphically sound, we are cautious about ascribing too much confidence to this age given that it is based on only two ^{10}Be ages.

The timing of formation of M_{AK4} is defined by a range of ages from 21.5 ± 0.7 to 15.1 ± 0.4 ka, with a corrected mean age of 16.1 ± 1.4 ka. The spread of ages for M_{AK4} and its position alongside adjacent hummocky moraine ridges may suggest that this moraine complex represents the gradual stabilization of glacial evidence during either a phase of glaciation or deglaciation.

With only two ^{10}Be exposure ages, 2.2 ± 1.4 and 1.6 ± 0.3 ka, and a weighted mean age of 1.6 ± 0.3 ka, the timing of formation for M_{AK3} cannot be well defined.

The timing of formation of M_{AK2} is defined by seven exposure ages, ranging from 27.6 ± 1.5 to 0.4 ± 0.03 ka. The corrected mean moraine age is 1.7 ± 1.5 ka when we eliminate the outlier age of 27.6 ± 1.5 ka (LATO1409). This outlier could be the result of the boulder's exposure to cosmic rays prior to the moraine formation.

The ^{10}Be boulder exposure ages for M_{AK1} range from 3.4 ± 0.3 to 0.2 ± 0.03 ka, with a corrected mean age of 0.3 ± 0.1 ka. This shows that M_{AK2} probably formed ~0.2 ka prior to M_{AK1}. The ^{10}Be ages of M_{AK1} and M_{AK2} demonstrate that the complex of moraine ridges at the terminus of the contemporary glacier (G_{AK1}) represents a succession of glacial advances and retreat phases over several hundred years.

B_{AK1} has bedrock exposure ages ranging from 14.4 ± 0.7 to 13.6 ± 0.6 ka, with a mean age of 13.9 ± 0.4 ka. This suggests that

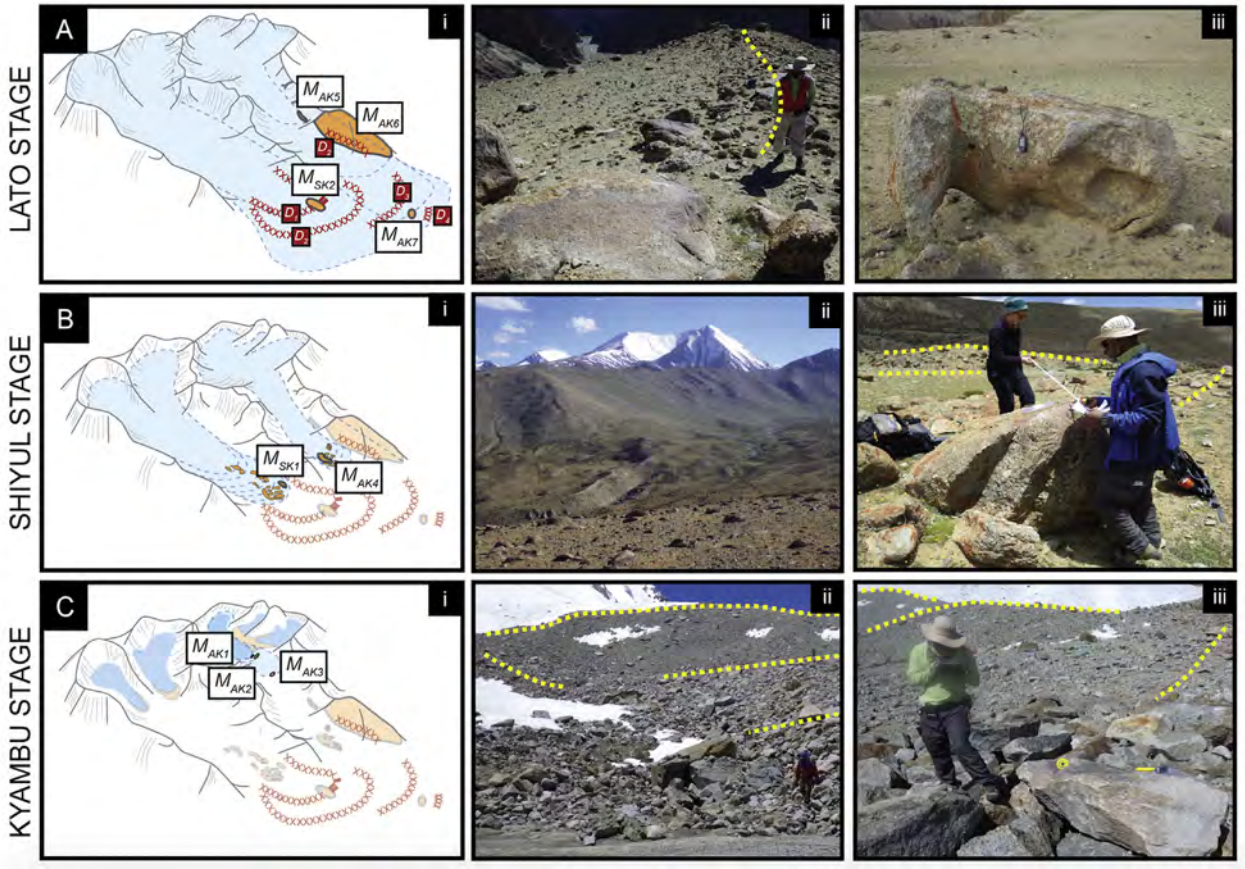

Fig. 4. Characteristics of local glacial stages in the Lato Massif. (A) Lato glacial stage. i) Schematic diagram of the glacial advances and till deposits of the Lato glacial stage. ii) M_{AK7} moraine ridge (ridges outlined by yellow dashed line herein). iii) Boulder with evidence of cavernous weathering from M_{AK7}. This boulder was not sampled for dating. (B) Shiyul glacial stage. i) Schematic diagram of the glacial advances of the Shiyul glacial stage. ii) M_{AK4} hummocky moraine complex. iii) Typical boulder (LATO-1429) on M_{AK4}. (C) Kyambu glacial stage. i) Schematic diagram of the glacial advances of the Kyambu glacial stage. ii) M_{AK1} and M_{AK2} complex. iii) Typical boulder (LATO-1411) on M_{AK2}. (For interpretation of the references to colour in this figure legend, the reader is referred to the Web version of this article.)

the ice retreated above ~5180 m asl within the valley at this time.

5.2. Starjuk Kangri study area

The ^{10}Be ages in the Starjuk Kangri valley are also consistent with the morphostratigraphy (Figs. 5 and 6; Tables 2 and 3). M_{SK2} has ages ranging from 98.7 ± 2.5 to 58.8 ± 5.5 ka, and a corrected mean age of 92.5 ± 6.7 ka.

Ages for M_{SK1} range from 25.8 ± 0.7 to 7.3 ± 0.4 ka, resulting in a corrected mean age of 22.4 ± 4.1 ka if we exclude sample ZK59 as an outlier because of its anomalously young age of 7.3 ± 0.4 ka. This outlier may be the result of boulder toppling, shielding or exhumation to the surface after the moraine formation.

5.3. Local glacial stages

The ^{10}Be chronology defines the timing of the Lato glacial stage to ~244–49 ka (marine isotope stage [MIS] 8–3), the Shiyul glacial stage to 25–15 ka (MIS 2), and the Kyambu glacial stage to 3.4–0.2 ka (MIS 1, middle–late Holocene). The contrasting geomorphic characteristics of the moraines including landform degradation and surface weathering for each of the glacial stages reflect the significant time differences between the glaciations (Tables 1 and 3). Other studies throughout the Himalayan-Tibetan orogen have defined glacial stages with durations exceeding 100 ka because of large uncertainties with subdividing very old glacial landforms. For example, Owen et al. (2012), for example identified four glacial stages within the Tashkurgan valley, southeast Pamir: the oldest of these (Dabudaer glacial stage) extending from 219 to 22 ka.

5.4. Till deposit chronology

The ^{10}Be chronostratigraphy and the moraine and till deposit morphostratigraphy indicate that the tills identified within the lower reaches of the valleys are likely to have been deposited before and during the Lato glacial stage (244–49 ka; Figs. 7 and 9). D_1 has been inset by the M_{SK1} and M_{SK2} moraines which date to 98.7 ± 2.5 ka, indicating that D_1 must be older than ~99 ka. D_2 has M_{SK2} inset into it and overlays the lower southern flank of the M_{AK6} moraine (113.3 ± 2.0–69.9 ± 2.9 ka). D_2 was therefore deposited between the formation of M_{SK1} and M_{SK2} and must therefore date to between MIS 5 and 3. The timing of deposition of D_3, which is downstream of D_2, must have occurred prior to 113.3 ± 2.0–69.9 ± 2.9 ka (the timing of formation of M_{AK6}), but following the formation of the M_{AK7} moraine (243.8±6–151.6 ± 6.4 ka). D_4 must have formed before 243.8 ± 6.0 ka, during MIS 8 or earlier as it underlies M_{AK7}.

6. ELA reconstructions

The contemporary glacier ELAs range between ~5520–5650 and ~5595–5600 m asl for the glaciers in the Amda Kangri ($G_{AK1\text{-}3}$) and Starjuk Kangri ($G_{SK1\text{-}3}$) valleys, respectively. These elevations fall within the uncertainties of, and marginally above the mean contemporary ELA of 5455 ± 130 m asl for the Ladakh and Zanskar

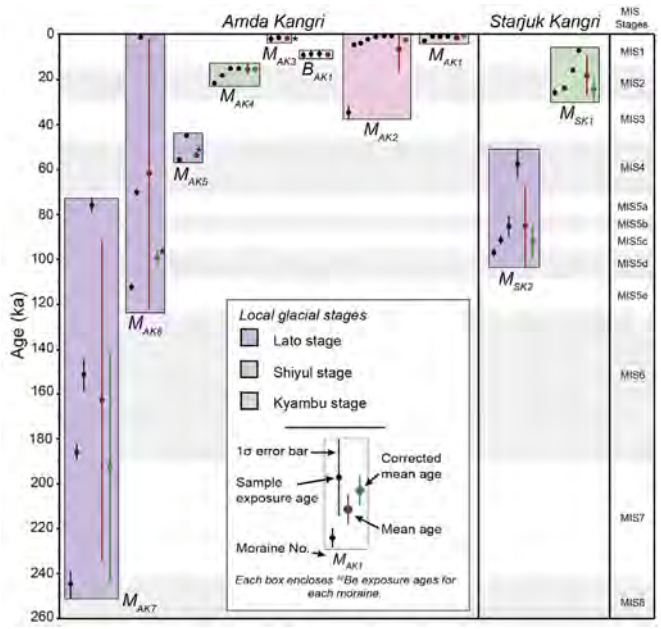

Fig. 5. Berylium-10 boulder exposure ages and mean ages for the moraines of the Lato study area (uncertainty expressed to 1σ). The corrected mean is the mean after outliers have been removed (* = weighted mean ages used when only two sample ages are assigned to the moraine). For each moraine, individual ages are plotted in descending order. Marine isotope stages from globally distributed benthic $\delta^{18}O$ records (Lisiecki and Raymo, 2005).

region (Dortch et al., 2011).

Glaciers in the Lato study area have retreated ~16 km upstream, ELAs increasing from ~5050 to 5650 m asl over the past 244 ka (Fig. 8, Table 4). There is a degree of overlap in the ELA ranges for the local glacial stages which can be explained by the inherent uncertainties associated with estimations of past glacier extents and hypsometry. Caution must therefore be exercised when interpreting the ELA values of this study.

The ELAs of the Lato glacial stage range between 5050 ± 130 and 5270 ± 130 m asl, with ΔELAs from 470 ± 140 to 250 ± 75 m. Partially coinciding with the Lato glacial stage, the Shiyul glacial stage has an ELA range of 5280 ± 70 to 5330 ± 105 m asl with an ΔELA of 270 ± 80 to 240 ± 70 m. This is because two of the Lato glacial stage moraines are situated upstream from the Shiyul glacial stage moraines.

The ELAs for the Kyambu glacial stage range between 5420 ± 50 and 5520 ± 20 m asl, with an ΔELA of 100 ± 30 m since ~3.4 ka. The resolution of the dating method, and the complicated arrangement of moraine ridges and undulating terrain make it difficult to determine whether M_{AK1} represents past, present or both glacial advances. The M_{AK1} moraine is considered representative of the maximum glacier extent of both the M_{AK1} glacial substage and the G_{AK1} contemporary glacier. This demonstrates that over the last ~300 years, the ELA of the Amda Kangri valley glacier has remained at ~5520 ± 20 m asl. The heights of the ice-contact moraines within this valley however, suggest that during this time, there has been a net loss to the glacier ice volume.

7. Discussion

The glacial chronostratigraphy for the Lato Massif consists of three local glacial stages, the Lato, Shiyul and Kyambu, including nine glacial substages ($M_{AK1\text{-}7}$, and $M_{SK1\text{-}2}$) extending back to at least to the last ~244 ka. Glaciations have changed from expanded ice caps, to large piedmont valley glaciers extending ~10 km downvalley, to cirque and small valley glaciers over the past three glaciations. This change in the pattern of glaciation has also been recognized within other Himalayan-Tibetan massifs such as the Gurla Mandhata (Owen et al., 2010), Muztag Ata and Kongur Shan (Seong et al., 2009a), and Tanggula Shan (Zheng and Jiao, 1991; Owen et al., 2005). These shifts in glacial style may be climatically controlled by means of a reduction of precipitation advancing over the interior of the orogen over the last few glacial cycles, effecting the moisture flux necessary to maintain positive glacier mass balances (Finkel et al., 2003; Bookhagen et al., 2005; Owen et al., 2008; Seong et al., 2009a). Alternatively, over several glacial cycles, the Lato Massif may have evolved from an isolated alpine plateau to a dissected and steep relief mountain range, where deep valleys were calved by geomorphic processes including glacial and fluvial erosion (Gilchrist et al., 1994; Naslund, 2001; Oskin and Burbank, 2005; Van der Beek and Bourbon, 2008). These changes to the landscape and the associated local climatic and environmental conditions may have been sufficient to influence the glaciation style over time (Owen et al., 2005, 2010). Why these shifts in glacial style are expressed within the study area has yet to be adequately explained. However, we favor regional climatic controls given the recurrent pattern of changes in glacial style over several glacial cycles, in many of the semi-arid regions of the

Table 3
Summary of the Lato study area moraine ages (uncertainty is expressed as 1σ). 1: Weighted mean ages calculated using methods described by Barrows, 2007) and Applegate et al. (2010, 2012). 2: Assigned ages are defined by the range of ^{10}Be ages of the moraines of each local glacial stage (not including outliers).

	No. of samples	Maximum age (ka)	Minimum age (ka)	Mean age (ka)	Corrected mean age (ka)	Weighted mean age[1] (ka)	Corrected weighted mean age[1] (ka)	Assigned age[2] (ka)
Lato stage								
M_{AK5}	2	57.3 ± 1.1	49 ± 1.8	–	–	55.2 ± 0.9	*	244–49
M_{SK2}	4	98.7 ± 2.5	58.8 ± 5.5	84.1 ± 17.7	92.5 ± 6.7[a]	92.0 ± 1.4	94.1 ± 1.4[a]	244–49
M_{AK6}	3	113.3 ± 2.0	1.1 ± 0.1	61.4 ± 56.6	–	1.6 ± 0.1	99.4 ± 1.7[b]	244–49
M_{AK7}	4	243.8 ± 6.0	75.2 ± 4.2	164.3 ± 70.5	194.0 ± 46.4[c]	162.2 ± 2.2	191.0 ± 2.5[c]	244–49
Shiyul stage								
M_{AK4}	4	21.5 ± 0.7	15.1 ± 0.4	17.4 ± 3.0	16.1 ± 1.4[d]	16.6 ± 0.2	16.1 ± 0.2[d]	25–15
M_{SK1}	4	25.8 ± 0.7	7.3 ± 0.4	18.6 ± 8.2	22.4 ± 4.1[e]	14.4 ± 0.3	23.8 ± 0.4[e]	25–15
Kyambu stage								
M_{AK1}	4	3.4 ± 0.3	0.2 ± 0.03	1.1 ± 1.6	0.3 ± 0.1[f]	0.3 ± 0.02	0.3 ± 0.02[f]	3.4–0.2
M_{AK2}	7	27.6 ± 1.5	0.4 ± 0.03	5.4 ± 9.9	1.7 ± 1.5[g]	0.5 ± 0.02	0.5 ± 0.02[g]	3.4–0.2
M_{AK3}	2	2.2 ± 1.4	1.6 ± 0.3	–	–	1.6 ± 0.3	*	3.4–0.2

–: Mean ages cannot be calculated because there are only two sample ages assigned to the moraine.
*: Corrected weighted mean age not necessary as no outliers were identified.
Excluded samples (a–g superscript) = a: ZK56; b: LATO1403; c: ZK53; d: LATO1428; e: ZK59; f: LATO1419; g: LATO1409.

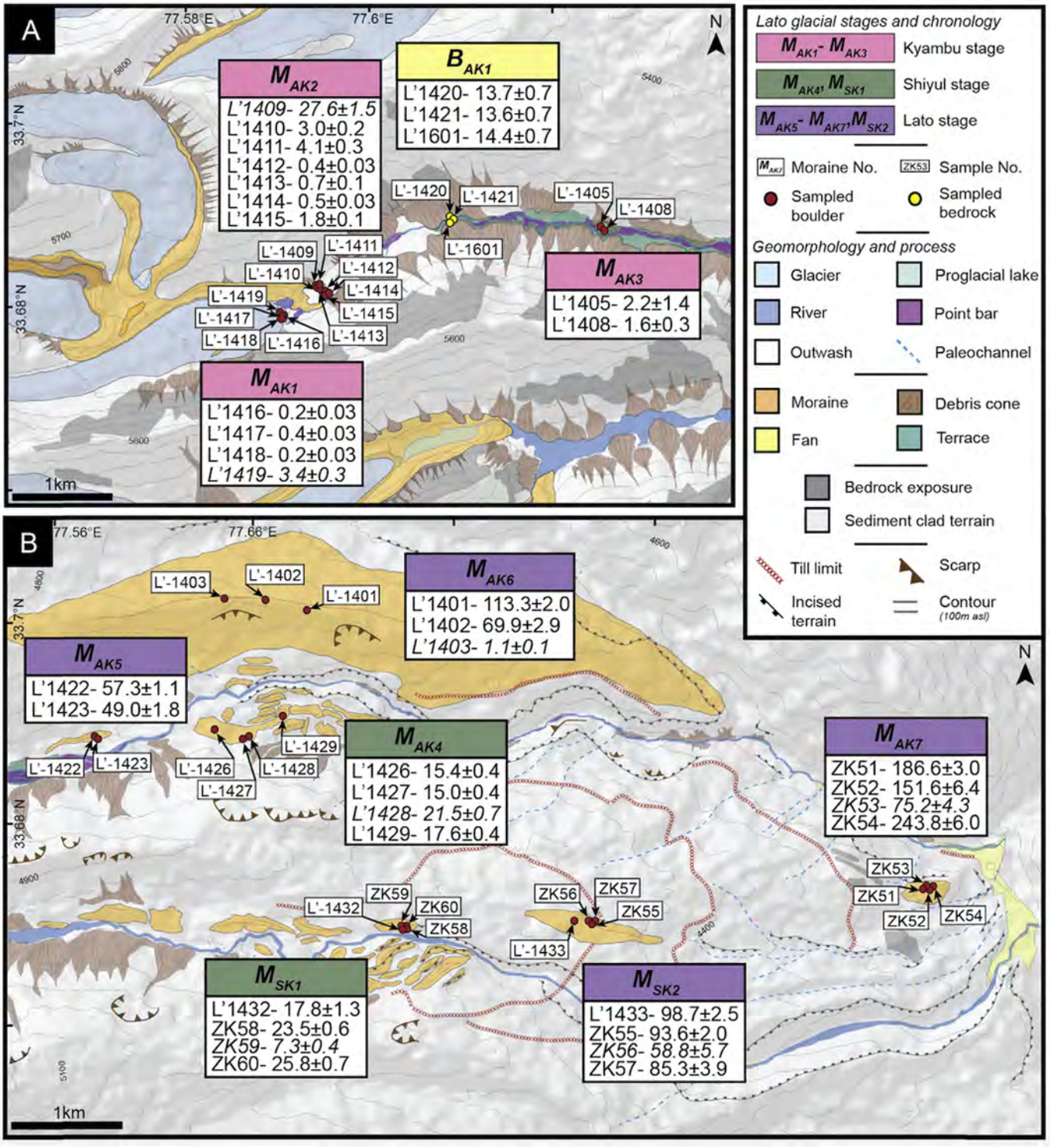

Fig. 6. Detailed geomorphology of the Lato study areas and ^{10}Be ages (ka) (Fig. 2 for location covered by maps). (A) Upper extent map showing the sample locations for each investigated moraine and bedrock surface, with the ^{10}Be exposure ages of the Kyambu glacial stage and B_{AK1}. (B) Lower extent map showing the sample locations for each investigated moraine with ^{10}Be exposure ages of the Shiyul and Lato stages. Identified outlier ages are italicized.

Himalayan-Tibetan orogen.

This pattern of progressively less extensive glaciation during the latter part of the Quaternary has been recognized in other mountain regions of world including, Tasmania, the Sierra Nevada, Alaska and the Peruvian Andes (Owen et al., 2010; Thackray et al., 2008; Owen and Dortch, 2014). Despite the complexities inherent within the Lato Massif glacial record, the Quaternary glaciations of this study area may even reflect a global pattern of glacial and climatic change.

Identifying the drivers of these glaciations and changes in style within the Lato Massif is challenging because of the uncertainties associated with the ^{10}Be dating (Owen and Dortch, 2014). Even with

the elimination of anomalously young and old ages, the Lato record still has a large spread of ^{10}Be ages for both the individual moraines/substages and the local glacial stages. Unlike other studies we are therefore unable to confirm that the Lato Massif glaciers responded to periods of increased monsoonal intensity (Owen et al., 2006; Dortch et al., 2010), or that the mid-latitude westerlies provided the dominant moisture source to maintain positive glacier mass balances (Dortch et al., 2013; Sharma et al., 2016). Nevertheless, our study provides the first step in defining the timing of glaciation in the region in order to enable us to begin to discuss the glacial history, paleoenvironmental change, and landscape evolution of the region.

As such, the characteristics, nature and significance of each glacial stage are discussed in the next three subsections.

7.1. Lato glacial stage

The Lato glacial stage includes four substages ($M_{AK5\text{-}7}$ and M_{SK2}), which extend from 244 to 49 ka over multiple glacial-interglacial cycles (Figs. 4A and 5; Table 3). Based upon morphostratigraphy alone, the moraines share very similar characteristics and yet record glacial advances of different ages. Therefore, despite the local stages being invaluable in describing the evolution of the study area, the glacial substages prove most useful when attempting to correlate the Lato record with local and regional studies.

The spread of ^{10}Be ages for the Lato glacial stage prevent this study from determining the exact ages of each substage and the factors that force glaciation. The surface weathering and shallow burial of some of the moraine boulders, and the possible input of boulders either fresh or with inheritance from the phases of till deposition during this stage may account for some of the scatter in the data. Although a higher resolution chronology would refine our conclusions, it remains clear that between ~244 and 150 ka, glaciers extended the full length of the Amda Kangri and Starjuk Kangri valleys. By the onset of the last glacial and the M_{AK6} substage (99.4 ± 1.4 ka), the glaciers had begun to retreat.

M_{AK6} is likely the product of multiple phases of formation over several glaciations and possibly even two or more glacial cycles. The description and position of M_{AK6} within the lower reaches of the Amda Kangri valley suggests that it may have been a lateral moraine for a glacier advance(s) that was greater in extent that the M_{AK7} advance, and extended into the Keylong-Leh valley. This would suggest that the primary formation of M_{AK6} occurred prior to ~244 ka, the ^{10}Be ages of this moraine defining the minimum age of its final formation phase.

The M_{SK2} (92.5 ± 6.7 ka) and M_{AK5} (55.2 ± 0.9 ka) substages provide further evidence of a retreating glacier margin during the early part of the last glacial (Fig. 9). With comparable surface weathering and landform degradation, M_{AK5} may be composed of reworked diamict from M_{AK6}. ^{10}Be ages could therefore either represent the timing of formation for M_{AK5}, or be the result of the complicated erosion and depositional history of M_{AK6}. This offers an explanation for the location of M_{AK5} on the hillslope rather than on the valley floor, and its preservation during the Shiyul glacial stage; a later glacial stage that extended beyond M_{AK5} downstream.

Although the glaciers are unlikely to have exceeded their valley limits, only high elevation tors and valley ridges were likely exposed above the ice during the Lato glacial stage. The Lato Massif likely supported a small ice cap/s with large outlet glaciers occupying its valleys during this glacial stage (Fig. 4A).

7.1.1. Lato glacial stage till deposits

The succession of till deposits in the lower reaches of the study areas are likely to have formed before and during the Lato glacial stage (244–47 ka) by glacial and paraglacial processes (Fig. 7). M_{AK7}, M_{SK1} and M_{SK2} overly some of these till deposits, suggesting low rates of landscape denudation and erosion during and after glaciation. These deposits probably represent ice-contact and resedimented glacial or paraglacial landforms formed by glacial outwash or outburst flood events. Based upon the size and distribution of the till deposits, it is possible that each deposit is a product of multiple depositional events.

7.2. Shiyul glacial stage

The Shiyul glacial stage has two substages, M_{AK4} and M_{SK1}, defined between ~25 and 15 ka during MIS 2 (Figs. 4B and 5). The moraine complexes represent fluctuating glacier margins possibly over a duration of ~12 ka in the valleys. Assigning these substages to climatostratigraphic events or defining possible drivers of glaciation at this time remains ambiguous.

The transition from the Lato to Shiyul glacial stages is different between the Amda Kangri and Starjuk Kangri valleys. Assuming that M_{AK5} is independent of M_{AK6}, the ELAs indicate that following

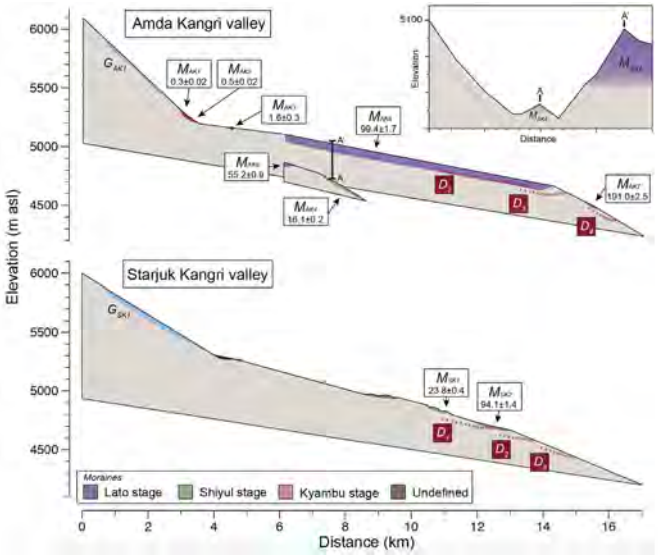

Fig. 7. Longitudinal profile of the Amda Kangri and Starjuk Kangri valleys with the mean ^{10}Be ages (ka) for each dated moraine. Red cross hatching indicates the location of the till deposits. (For interpretation of the references to colour in this figure legend, the reader is referred to the Web version of this article.)

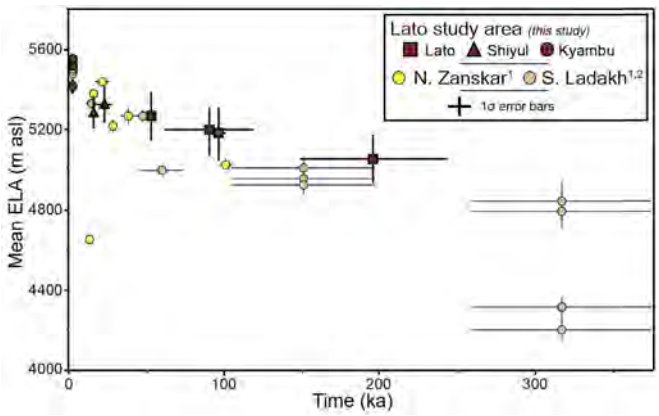

Fig. 8. Mean ELAs (±stdev) for the Lato study area glacial substages (grouped by local stage) and local glacial stages of the northern Zanskar (1 = Orr et al., 2017) and southern Ladakh Ranges (2 = Owen et al., 2006).

Table 4
Reconstructed ELAs (uncertainty is expressed as 1σ) for Lato study area.[a]

	Glacier area	Glacier head	Glacier toe	Aspect	Area-Altitude	Area-Accumulation ratio			Toe-Headwall altitude ratio		Mean ELA	ELA depression
	(~km^2)	(m asl)	(m asl)		AA	AAR(0.4)	AAR(0.5)	AAR(0.6)	THAR(0.4)	THAR(0.5)	(m asl)	(m)
Amda Kangri valley												
Contemporary glaciers												
$G_{AKpres1}$	2	5770	5330	ENE	5530	5540	5520	5490	5500	5545	5520 ± 20	–
$G_{AKpres2}$	2	5785	5555	ESE	5650	5670	5660	5650	5620	5645	5650 ± 20	–
$G_{AKpres3}$	3	6000	5510	SSE	5650	5670	5660	5650	5625	5650	5650 ± 15	–
Kyambu glacial stage												
M_{AK1}	2	5770	5330	ENE	5526	5540	5520	5490	5500	5545	5520 ± 20	–
M_{AK2}	4	5770	5275	ENE	5520	5550	5520	5490	5480	5535	5515 ± 30	5 ± 1.5
M_{AK3}	14	5770	5110	ENE	5420	5470	5400	5340	5400	5480	5420 ± 50	100 ± 30
Shiyul glacial stage												
M_{AK4}	37	5785	4790	ENE	5275	5330	5250	5180	5270	5385	5280 ± 70	240 ± 70
Lato glacial stage												
M_{AK5}	17	5785	4900	ENE	5040	5360	5280	5230	5300	5405	5270 ± 130	250 ± 75
M_{AK6}	123	5785	4280	ENE	5230	5380	5250	5120	4965	5155	5180 ± 140	340 ± 100
M_{AK7}	98	5785	4120	ENE	5090	5240	5110	4970	4850	5050	5050 ± 130	470 ± 140
Starjuk Kangri valley												
Contemporary glaciers												
$G_{SKpres1}$	5	5755	5290	ENE	5620	5650	5630	5610	5525	5585	5600 ± 45	–
$G_{SKpres2}$	7	5825	5290	N	5595	5630	5580	5560	5535	5595	5580 ± 30	–
$G_{SKpres3}$	2	5845	5355	N	5605	5650	5610	5580	5535	5590	5595 ± 40	–
Shiyul glacial stage												
M_{SK1}	29	5550	4820	ENE	5320	5470	5340	5160	5280	5395	5330 ± 105	270 ± 80
Lato glacial stage												
M_{SK2}	32	5550	4575	ENE	5220	5360	5150	5030	5110	5255	5190 ± 115	410 ± 125

[a] ELAs rounded to the nearest multiple of five.

the retreat of ice during the Lato glacial stage in the Amda Kangri valley, the glaciers readvanced during and prior to the Shiyul glacial stage. This readvance is not evident within the Starjuk Kangri valley, where the chronostratigraphy and glacial evidence illustrates the continued retreat of ice through the Lato glacial stage and to the Shiyul glacial stage. However, if M_{AK5} is reworked from M_{AK6}, then the transition from Lato to Shiyul glacial stages in both valleys can be considered comparable. The location and elevation of the moraine complexes in the widening floor of each valley suggest that the Shiyul glacial stage records a shift in glaciation style away from a small ice cap/s to one of large alpine valley glaciers (Fig. 4B).

Moraines of the Shiyul glacial stage overly the D_1 till deposit indicating that following the Lato glacial stage, the valley glaciers covered and eroded the till, likely removing and redistributing some of the sediment. Some of this till may have been reworked and deposited as hummocky moraines during the Shiyul glacial stage. The tills of the study area are likely to have been further incised as part of the landscape readjustment to the climatic and environmental conditions associated with this glacial stage.

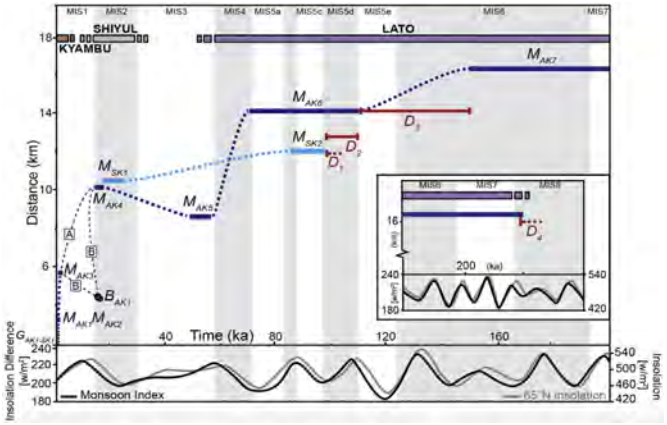

Fig. 9. Time-distance diagram (distance from the contemporary glacier snout: $G_{AK1\text{-}SK1}$) for the glacial stages, glacial substages and relative timing of till deposition of the Lato study area. Dashed blue lines denote estimated glacier extents over time: Dark blue = Amda Kangri glacier; Light blue = Starjuk Kangri glacier. Red lines denote minimum timing of till deposition. Between M_{AK3} and M_{AK4}: Path A marks the retreat of ice between the Shiyul and Kyambu glacial stages as proposed by Saha et al. (2018). Path B marks the retreat and readvance of ice between the Shiyul and Kyambu glacial stages indicated by the chronostratigraphy and bedrock exposure ages of this study. Plot is compared to the simulated monsoonal index and 65°N insolation of Leuschner and Sirocko (2003). Marine isotope stages are drawn from Lisiecki and Raymo (2005) globally distributed benthic $\delta^{18}O$ records. (For interpretation of the references to colour in this figure legend, the reader is referred to the Web version of this article.)

7.3. Kyambu glacial stage

The Kyambu glacial stage has three glacial substages (M_{AK1-3}) between ~3.4 ka and 0.2 ka (Figs. 4C and 5). The B_{AK1-3} ages (14.4 ± 0.7–13.6 ± 0.7 ka) within this stretch of the Amda Kangri valley demonstrate that following the Shiyul glacial stage, and prior to the Kyambu glacial stage, the glacial ice retreated to within ~2 km of the present glacier (G_{AK1}). M_{AK3} marks the first substage of the Kyambu glacial stage, when a glacier advanced over these bedrock surfaces. The glacier that advanced during this time was probably not sufficiently erosive to exhume bedrock deep enough to reset the ages of the surfaces. The consistency between the bedrock ages is indicative of either uniform erosion across the bedrock surface or more likely, little-no erosion. This would explain why the ages are older than the glacier advances during the Kyambu glacial stage. Despite evidence of some glacial polish at the sampling site, the low erosion rates within this region make it highly unlikely that more than 60 cm of bedrock would have been removed during the Kyambu glacial stage (Dietsch et al., 2015). The weathering and polish of the bedrock surfaces is therefore likely to be a product of the last few glacial stages. However, with only two ^{10}Be ages to define the age of M_{AK3}, and its proximity to the hillslopes and talus deposits, it is important to acknowledge that the landform or sampled boulders may not be representative of a Holocene glacier advance. Based upon the Holocene record alone, Saha

et al. (2018) has proposed that the ages assigned to M_{AK3} possibly reflect later depositional events. The initial formation age of M_{AK3} may therefore predate the bedrock exposure ages (14.4 ± 0.7–13.6 ± 0.7 ka). This would possibly mean that the glacier did not readvance within the Amda Kangri valley between 13.6 ± 0.7 ka and the onset of the Kyambu stage. Moreover, this would mean that the Kyambu glacial stage would include glacier advances from and prior to, the Holocene. We are confident however that this moraine marks the onset of the Kyambu glacial stage based upon the sedimentology and geomorphic descriptions of M_{AK3} and the boulder samples, and that the ^{10}Be ages should not be ignored.

By the late Holocene, the glaciers had retreated to within ~500 m of the contemporary glacier limits. The M_{AK1} and M_{AK2} complex is characteristic of late Holocene glacial landforms in the Himalaya by being slightly weathered and unstable (Owen, 2009). The timing of the Kyambu glacial stage broadly coincides with a period of reduced monsoonal intensity and insolation (Figs. 8 and 9). This possibly explains the rapid retreat of glaciers during this time.

The Kyambu glacial stage marks another shift in glaciation style, from large valley glaciers during the Shiyul glacial stage to small valley and cirque glaciers of today. The Holocene record has a better potential to preserve evidence for centennial timescale glacier oscillations because of a greater preservation potential than older moraines (Owen, 2009; Saha et al. 2018).

7.4. Local and regional significance

The spread of ^{10}Be ages for the ^{10}Be chronostratigraphy and the uncertainties associated with the reconstructed ELAs for the Lato Massif prevent the glacial substages and stages of this record from being statistically correlated with other local and regional stages for the NW Himalaya (Fig. 10).

M_{AK7} represents the oldest and most extensive glaciation of the Lato glacial stage (ELA: 5050 ± 130 m asl), and may correlate with the Deshkit 3 (156 ± 16 ka; Dortch et al., 2010) and Kar (151 ± 46 ka; ELA: 5020 ± 56 m asl; Owen et al., 2006; Orr et al., 2017) local glacial stages of the Ladakh Range, and regional SWHTS stage 6 (146 ± 18 ka; Dortch et al., 2013). Although these glacial stages cannot be considered synchronous, this does suggest a regional pattern of major glaciation during MIS 6.

Based upon the size and morphology of M_{AK6}, and the reconstructed ELAs (5180 ± 140 m asl) at 99.4 ± 1.4 ka, parallels can be drawn between this glacial substage and the Leh (ELA: 4795 ± 81 m asl, 317 ± 57 ka) and KM0 (311 ± 8 ka) glacial stages of the Ladakh (Owen et al., 2006) and Zanskar (Hedrick et al., 2011) ranges, respectively. The ^{10}Be ages of M_{AK6} are likely to represent minimum ages of the final depositional event of this moraine's formation, with initial development possibly coinciding with the Leh and KM0 glacial stages.

The Shiyul glacial stage and its substages may be coincident with several local stages in the northern Zanskar (M_{G2-3}, M_{S3}; Orr et al., 2017) and Ladakh ranges (Ladakh-2; Dortch et al., 2013). The corresponding moraines within these regions have single or multiple clear crests, in contrast to the hummocky moraine complexes of the Shiyul glacial stage. The morphology of the moraines for the Shiyul glacial stage has been used in this study as evidence of fluctuating glacier margins over millennial timescales. A similar moraine complex has been identified within the massif, to the southeast of the Lato study area. The timing of its formation is unknown. The Lato Massif may therefore have provided the necessary climatic and geologic conditions to facilitate this style and succession of glaciation at this time. An alternative explanation is that these hummocky moraine complexes are poorly preserved in the glacial record.

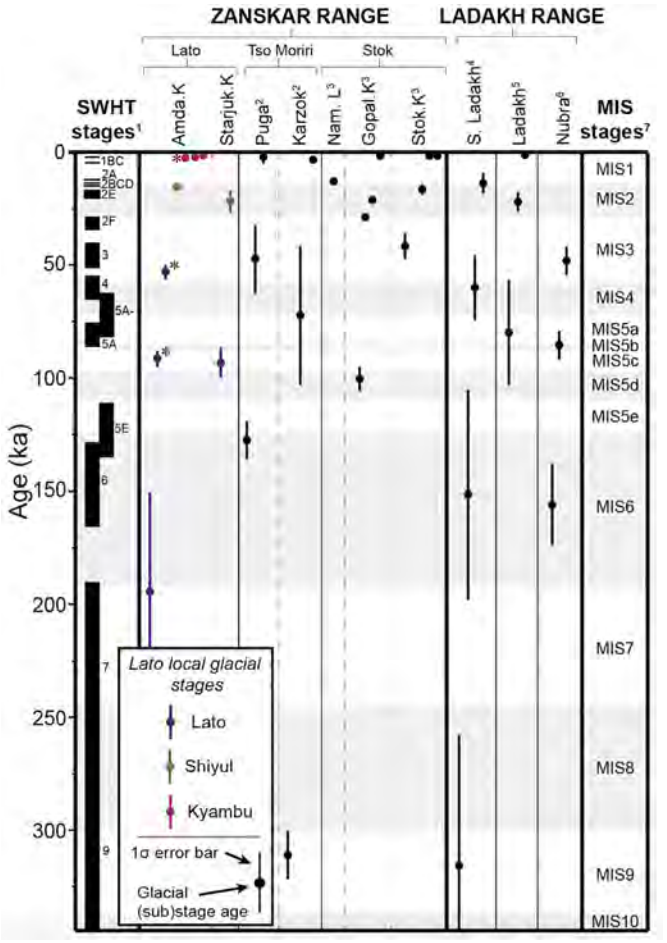

Fig. 10. Lato study area glacial chronology (corrected mean age of glacial substages) with local and regional glacial chronologies (* = weighted mean ages used when only two sample ages are assigned to the moraine). Semi-arid western Himalayan-Tibetan glacial stages (SWHTS) regional glacial stages from (1) Dortch et al. (2013). Zanskar Range chronologies from (2) Tso Moriri (Hedrick et al., 2011) and (3) Stok (Orr et al., 2017). Ladakh Range chronologies from (4) southern Ladakh (Owen et al., 2006), (5) northern Ladakh (Dortch et al., 2013) and (6) Nubra (Dortch et al., 2010). Marine isotope stages are drawn from Lisiecki and Raymo (2005) globally distributed benthic δ^{18}O records.

The glacier margins of the Lato study area have fluctuated significantly within the last ~3.4 ka. This is consistent with local and regional glacial records of late Holocene glaciations (Saha et al., 2018). There is also no evidence of glacier advances between ~50 and 30 ka. Whether the glaciers were less extensive during this time or that the glacial evidence has been removed or reworked is not known.

Previous or more extensive glaciations may have extended into the Keylong-Leh valley in the past as the valley morphology and the moraine and till deposit morphostratigraphy suggests. The evidence for previous glaciations may have then been obscured by the deposition of younger sediments and/or removed by erosion. This is supported by evidence of glacial stages much older throughout the region, than those recorded within the Lato Massif (Fig. 10; Owen et al., 2006; Hedrick et al., 2011; Dortch et al., 2013).

7.5. Lato Massif till deposits

The Lato Massif till deposits are similar to other thick valleys fill deposits throughout many valleys in the Himalayan-Tibetan

orogen. Many of these thick valley fills represent resedimentation during times of deglaciation (Barnard et al., 2004, 2006). Till deposits consistent with those of this study are evident on Google Earth images of the northern most extent and eastern and southwestern flanks of the Lato Massif (Fig. 11). In each case, the till deposits extend to the lower elevations of the respective valleys, and are preserved alongside evidence of past and present glaciation, although their genesis is unclear.

The large successions of tills are located within the eastern sector of the massif, where resistant granites, orthogneisesses and Mesozoic-Paleozoic sedimentary rocks are present (Fig. 1). The western valleys with limited till preservation are characterized by a combination of less resistant Paleozoic-Precambrian sedimentary formations. This suggests that factors other than lithology play primary roles in the deposition and preservation of these deposits. The development of till chronostratigraphies through numerical dating would help to solidify our understanding of the erosion and sedimentation of the landscapes of this study area.

The thick till deposits at the mouths of the study areas may represent times of localized incision and sediment flux controlled by glacial processes (Barnard et al., 2004, 2006; Dortch et al., 2011). This offers an explanation for why the east and southwest flanks of the massif, with less extensive late Quaternary glaciation have retained similar till deposits (Fig. 11). These small and highly incised valleys may have restricted the preservation of glacial evidence and aided the more efficient evacuation of sediment from within its valleys. The locations of the successions of moraines suggest that glaciers would have been predominately confined to the upper valley elevations. This suggests that the Lato Massif may have supported an asymmetrical ice cap during the Lato glacial stage, with more restricted glaciation on the western flank of the massif, and large outlet glaciers extending the full length of the valleys on the eastern flank. More detailed mapping of the eastern flank would help to better our understanding of the glacial history of the Lato Massif and central Zanskar.

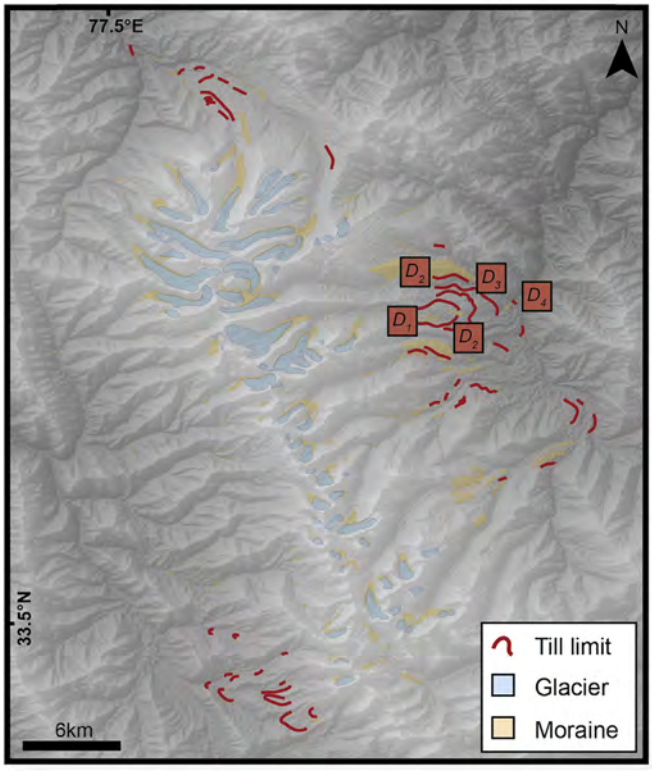

Fig. 11. Map of the Lato Massif till limits overlying an ASTER DEM. Till limits of the Lato study area are highlighted (D_1-D_4).

8. Conclusion

Three major glacial stages, the Lato, Shiyul and Kyambu, within the Lato Massif, are evident in our study area extending back to ~244 ka. These glacial stages include 9 glacial substages (M_{AK1}–M_{AK7}, M_{SK1}–M_{SK2}). Each glaciation becomes progressively less extensive in the Lato Massif over time.

The Lato glacial stage is the oldest (244–49 ka) and most extensive period of glaciation within the Lato Massif, where large outlet glaciers likely sourced from a small ice cap extended the full length of the valleys. Large till deposits associated with this stage are evident at the valley mouths. The Shiyul glacial stage (25–15 ka) represents a shift in glacial style from large outlet glaciers to smaller valley glaciers. By the middle to late Holocene, during the Kyambu glacial stage (3.4–0.2 ka), glaciers became restricted to the cirques and headwalls of the massif. This study joins others from the Himalaya and Tibet where major shifts in glaciation style of this kind have been recognized (Seong et al., 2009a; Owen et al., 2010). This suggests that the pattern of glaciation may reflect regional climatic forcing. A possibility is that over several glacial-interglacial cycles, the Lato Massif evolved from an isolated alpine plateau to a steep relief mountain range through erosive geomorphic processes, forcing a shift in glaciation style from small ice cap to entrenched valley and cirque glaciers (Owen et al., 2005).

The resolution of the glacial geologic record in the Lato Massif does not allow us to adequately identify the primary local or regional forcing important in influencing the glacial style and landscape development of the region. Despite these challenges, the ^{10}Be chronostratigraphy offers the first step into defining the timing and controls of Quaternary glaciation for central Zanskar. The geomorphic mapping and ^{10}Be chronology show that the landscape evolution of the study area and the wider Lato Massif has occurred over multiple glacial-interglacial cycles through glacial, paraglacial and fluvial processes.

Our study shows that despite the close proximity of the study area to preexisting glacial records within the Zanskar and Ladakh ranges, the timing and duration of the glacial chronologies vary significantly. This supports the view that localized climatic, environmental and geological conditions play a principle role in governing the nature and timing of glaciation within these Himalayan alpine settings.

Building upon this chronostratigraphy and examining the glacial histories of some additional valleys of the Lato Massif would help better explore the shifting styles of glaciation within the Zanskar Range and Transhimalaya. This would also enable the better comparison of the timing and drivers of late Quaternary glaciation within and between the semi-arid mountain ranges of the NW Himalaya and beyond.

Acknowledgments

ENO, LAO, SS and MKM would like to thank the Department of Geology at the University of Cincinnati for fieldwork support and for the processing of samples for ^{10}Be dating in the geochronology laboratory facilities. ENO and SS thank the Geological Society of America for Graduate Student Research Grants and the Graduate Student Governance Association, University of Cincinnati for research fellowships to conduct fieldwork. MWC acknowledges support from NSF (EAR-1560658). Many thanks to Editor Neil Glasser and two anonymous reviewers for their very constructive comments that helped us revise our manuscript.

Appendix A. Supplementary data

Supplementary data related to this article can be found at https://doi.org/10.1016/j.quascirev.2018.01.005.

References

Ali, S., Biswas, R., Shukla, A., 2013. Chronology and climatic implications of Late Quaternary glaciations in the Goriganga valley, central Himalaya, India. Quat. Sci. Rev. 73, 59–76.

Applegate, P., Urban, N., Laabs, B., Keller, K., Alley, R., 2010. Modeling the statistical distributions of cosmogenic exposure dates from moraines. Geosci. Model Dev. 3, 293–307.

Applegate, P., Urban, N., Keller, K., Lowell, T., Laabs, B., Kelly, M., Alley, R., 2012. Improved moraine age interpretations through explicit matching of geomorphic process models to cosmogenic nuclide measurements from single landforms. Quat. Res. 77 (2), 293–304.

Balco, G., Stone, J., Lifton, N., Dunai, T., 2008. A complete and easily accessible means of calculating surface exposure ages or erosion rates from ^{10}Be and ^{26}Al measurements. Quat. Geochronol. 3, 174–195.

Barnard, P., Owen, L., Finkel, R., 2004. Style and timing of glacial and paraglacial sedimentation in a monsoon-influenced high Himalayan environment, the upper Bhagirathi Valley, Garhwal Himalaya. SE. Geol. 165, 199–221.

Barnard, P., Owen, L., Finkel, R., Asahi, K., 2006. Landscape response to deglaciation in a high relief, monsoon-influenced alpine environment, Langtang Himal, Nepal. Quat. Sci. Rev. 25, 2162–2176.

Barrows, T.T., 2007. Absence of cooling in New Zealand. Geology 86, 86–89.

Benn, D., Owen, L., 1998. The role of the Indian summer monsoon and the mid-latitude westerlies in Himalayan glaciation: a review and speculative discussion. J. Geol. Soc. 155, 353–363.

Benn, D.I., Owen, L.A., 2002. Himalayan glacial sedimentary environments: a framework for reconstructing and dating former glacial extents in high mountain regions. Quat. Int. 97-98, 3–26.

Benn, D., Owen, L., Osmaston, H., Seltzer, G., Porter, S., Mark, B., 2005. Reconstruction of equilibrium-line altitudes for tropical and sub-tropical glaciers. Quat. Int. 138-139, 8–21.

Bhutiyani, M., 1999. Mass-balance studies on siachen glacier in the Nubra valley, karakorum Himalaya, India. J. Glaciol. 45, 112–118.

Bolch, T., Kulkarni, A., Kaab, A., 2012. The state and fate of Himalayan glaciers. Science 336, 310–314.

Bookhagen, B., Burbank, D., 2006. Topography, relief and TRMM-derived rainfall variations along the Himalaya. Geophys. Res. Lett. 33, 105.

Bookhagen, B., Burbank, D., 2010. Toward a complete Himalayan hydrological budget: spatiotemporal distribution of snowmelt and rainfall and their impact on river discharge. J. Geophys. Res. 115 (F3), 1–25.

Bookhagen, B., Thiede, R., Strecker, M., 2005. Late Quaternary intensified monsoon phases control landscape evolution in the northwest Himalaya. Geology 33 (1), 149–152.

Brozovic, N., Burbank, D.W., Meigs, A.J., 1997. Climatic limits on landscape development in the northwestern Himalaya. Science 276, 571–574.

Burbank, D., Blythe, A., Putkonen, J., Pratt-Sitaula, B., Gabet, E., Oskin, M., Barros, A., Ojha, T., 2003. Decoupling of erosion and precipitation in the Himalayas. Nature 426, 652–655.

Clark, P.U., Dyke, A.S., Shakun, J.D., Carlson, A.E., Clark, J., Wohlfarth, B., Mitrovica, J.X., Hostetler, S.W., McCabe, A.M., 2009. The last glacial maximum. Science 325, 710–714.

Damm, B., 2006. Late quaternary glacier advances in the upper catchment area if the Indus River (Ladakh and western Tibet). Quat. Int. 154-155, 87–99.

Derbyshire, E., Shi, Y., Li, J., Zheng, B., Li, S., Wang, J., 1991. Quaternary glaciation of Tibet: the geological evidence. Quat. Sci. Rev. 10, 485–510.

Dietsch, C., Dortch, J., Reynhout, S., Owen, L., Caffee, M., 2015. Very slow erosion and topographic evolution of the Southern Ladakh range. India. Earth Surf. Proc. Land 40 (3), 389–402.

Dortch, J.M., Owen, L.A., Haneberg, W.C., Caffee, M.W., Dietsch, C., Kamp, U., 2009. Nature and timing of mega-landslides in northern India. Quat. Sci. Rev. 28, 1037–1056.

Dortch, J., Owen, L., Caffee, M., 2010. Quaternary glaciation in the Nubra and Shyok valley confluence, northernmost Ladakh, India. Quat. Res. 74, 132–144.

Dortch, J., Owen, L., Schoenbohm, L., Caffee, M., 2011. Asymmetrical erosion and morphological development of the central Ladakh Range, northern India. Geomorphology 135, 167–180.

Dortch, J., Owen, L., Caffee, M., 2013. Timing and climatic drivers for glaciation across semi-arid western Himalayan-Tibetan orogen. Quat. Sci. Rev. 78, 188–208.

Finkel, R., Owen, L., Barnard, P., Caffee, M., 2003. Beryllium-10 dating of Mount Everest moraines indicates a strong monsoon influence and glacial synchroneity throughout the Himalaya. Geology 31 (6), 561–564.

Gilchrist, A., Summerfield, M., Cockburn, H., 1994. Landscape dissection, isostatic uplift, and the morphologic development of orogens. Geology 22 (11), 963–966.

Hedrick, K., Seong, Y., Owen, L., Caffee, M., Dietsch, C., 2011. Towards defining the transition in style and timing of Quaternary glaciation between the monsoon-influenced Greater Himalaya and the semi-arid Transhimalaya of Northern India. Quat. Int. 236, 21–33.

Heyman, J., 2014. Paleoglaciation of the Tibetan Plateau and surrounding mountains based on exposure ages and ELA depression estimates. Quat. Sci. Rev. 91, 30–41.

Heyman, J., Stroeven, A., Harbor, J., Caffee, M., 2011. Too young or too old: evaluating cosmogenic exposure dating based on an analysis of compiled boulder exposure ages. Earth Planet Sci. Lett. 302, 71–80.

Hobley, D., Sinclair, H., Cowie, P., 2010. Processes, rates, and timescales of fluvial response in an ancient postglacial landscape of the northwest Indian Himalaya. Geol. Soc. Am. Bull. 122, 1569–1584.

Hughes, P., 2010. Geomorphology and Quaternary Stratigraphy: the roles of morpho-, litho- and allostratigraphy. Geomorphology 123, 189–199.

Hughes, P., Gibbard, P., Woodwad, J., 2005. Quaternary glacial records in mountain regions: a formal stratigraphical approach. Episodes 28, 85–92.

Ivy-Ochs, S., Kerschner, H., Schlüchter, C., 2007. Cosmogenic nuclides and the dating of Lateglacial and Early Holocene glacier variations: the Alpine perspective. Quat. Int. 164–165, 53–63.

Jonell, T.N., Owen, L.A., Carter, A., Schwenniger, J.-L., Clift, P.D., 2018. Quantifying episodic erosion and transient storage on the western margin of the Tibetan Plateau, upper Indus river. Quat. Res. 89, 281–306.

Korup, O., Montgomery, D.R., 2008. Tibetan plateau river incision inhibited by glacial stabilization of the Tsangpo gorge. Nature 455, 786–789.

Lee, S.Y., Seong, Y.B., Owen, L. a., Murari, M.K., Lim, H.S., Yoon, H. Il, Yoo, K.C., 2014. Late Quaternary glaciation in the Nun-Kun massif, northwestern India. Boreas 43, 67–89.

Leuschner, D., Sirocko, F., 2003. Orbital insolation forcing of the Indian Monsoon- a motor for global climate changes? Paleogeo. Paleoclim. Paleoecol 197, 83–95.

Lifton, N., Sato, T., Dunai, T., 2014. Scaling in situ cosmogenic nuclide production rates using analytical approximations to atmospheric cosmic-ray fluxes. Earth Planet Sci. Lett. 386, 149–160.

Lisiecki, L., Raymo, M., 2005. A Pliocene-Pleistocene stack of 57 globally distributed benthic δ18O records. Paleocean 20, 1.

Marrero, S., Philips, F., Borchers, B., Lifton, N., 2016. Cosmogenic nuclide systematics and the CRONUScale program. Quat. Geochronol. 31, 1–72.

Martin, L., Blard, P., Balco, G., Laurent, V., 2017. The CREp program and the ICE-D production rate calibration database: a fully parameterizable and updated online tool to compute cosmic-ray exposure ages. Quat. Geochronol. 38, 25–49.

Mitchell, W., Taylor, P., Osmaston, H., 1999. Quaternary geology in Zanskar, NW Indian Himalaya: evidence of restricted glaciation and preglacial topography. J. Asian Earth Sci. 307–318.

Molnar, P., England, P., 1990. Late Cenozoic uplift of mountain ranges and global climatic change: chicken or egg? Nature 46, 29–34.

Nagar, Y., Ganju, A., Satyawali, P., 2013. Preliminary optical chronology suggests significant advance in Nubra valley glaciers during the last glacial maximum. Curr. Sci. 105, 96–101.

Naslund, J., 2001. Landscape development in western and central dronning maud land, east Antarctica. Antarct. Sci. 13 (3), 302–311.

Orr, E., Owen, L., Murari, M., Saha, S., Caffee, M., 2017. The timing and extent of Quaternary glaciation of Stok, northern Zanskar Range, Transhimalaya, of northern India. Geomorphology 284, 142–155.

Oskin, M., Burbank, D., 2005. Alpine landscape evolution dominated by cirque retreat. Geology 33 (12), 933–936.

Osmaston, H., 1994. The geology, geomorphology and quaternary history of zangskar in crook J. In: Osmaston, H. (Ed.), Himalayan Buddhist Villages, pp. 1–35. Chapt 1.

Osmaston, H., 2005. Estimates of glacier equilibrium line altitudes by the area × altitude, the area × altitude balance ratio and the area × altitude balance index methods and their validation. Quat. Int. 138–139, 22–31.

Owen, L., 2009. Latest Pleistocene and Holocene glacier fluctuations in the Himalaya and Tibet. Quat. Sci. Rev. 28, 21–22, 2150-2164.

Owen, L., Dortch, J., 2014. Nature and timing of Quaternary glaciation in the Himalayan-Tibetan orogen. Quat. Sci. Rev. 88, 14–54.

Owen, L.A., Finkel, R.C., Barnard, P.L., Ma, H., Asahi, K., Caffee, M.W., Derbyshire, E., 2005. Climatic and topographic controls on the style and timing of Late Quaternary glaciation throughout Tibet and the Himalaya defined by ^{10}Be cosmogenic radionuclide surface exposure dating. Quat. Sci. Rev. 24, 1391–1411.

Owen, L., Caffee, M., Bovard, K., Finkel, R., Sharma, M., 2006. Terrestrial cosmogenic nuclide surface exposure dating of the oldest glacial successions in the Himalayan orogen: Ladakh Range, northern India. GSA Bull. 118, 3–4, 383-392.

Owen, L.A., Caffee, M.W., Finkel, R.C., Seong, B.S., 2008. Quaternary glaciation of the Himalayan–Tibetan orogen. J. Quat. Sci. 23, 513–532.

Owen, L.A., Chaolu, Yi, Finkel, R., Davis, N., 2010. Quaternary glaciation of Gurla Mandhata (Naimon'anyi). Quat. Sci. Rev. 29, 1817–1830.

Owen, L., Chen, J., Hedrick, K., Caffee, M., Robinson, A., Schoenbohm, L., Yuan, Z., Li, W., Imrecke, D., Liu, J., 2012. Quaternary glaciation of the Tashkurgan valley, southeast Pamir. Quat. Sci. Rev. 47, 56–72.

Putkonen, J., Connolly, J., Orloff, T., 2008. Landscape evolution degrades the geologic signature of past glaciations. Geomorphology 97, 208–217.

Putnam, A.E., Schaefer, J.M., Denton, G.H., Barrell, D.J.A., Birkel, S.D., Andersen, B.G., Kaplan, M.R., Finkel, R.C., Schwartz, R., Doughty, A.M., 2013. The last glacial maximum at 44°S documented by a ^{10}Be moraine chronology at lake Ohau, southern Alps of New Zealand. Quat. Sci. Rev. 62, 114–141.

Saha, S., Owen, L., Orr, E., Caffee, M., 2018. Timing and nature of Holocene glacial advances at the northwestern end of the Himalayan-Tibetan orogen. Quat. Sci. Rev. (in revisions).

Schlup, M., Carter, A., Cosca, M., Steck, A., 2003. Exhumation history of eastern Ladakh revealed by 40Ar/39Ar and fission-track ages: the Indus River- Tso

morari transect, NW Himalayas. J. Geol. Soc. 160, 385–399.
Searle, M., 1986. Structural evolution and sequence of thrusting in the high Himalayan, Tibetan-Tethys and Indus suture zones of zanskar and Ladakh, western Himalaya. J. Struct. Geol. 8 (8), 923–936.
Seong, Y.B., Owen, L.A., Bishop, M.P., Bush, A., Clendon, P., Copland, L., Finkel, R., Kamp, U., Shroder, J.F., 2007. Quaternary glacial history of the central karakoram. Quat. Sci. Rev. 26, 3384–3405.
Seong, Y.B., Owen, L.A., Bishop, M.P., Bush, A., Clendon, P., Copland, P., Finkel, R., Kamp, U., Shroder, J.F., 2008. Reply to comments by matthias kuhle on "Quaternary glacial history of the central karakoram". Quat. Sci. Rev. 27, 1656–1658.
Seong, Y.B., Owen, L.A., Yi, Chaolu, Finkel, R., 2009a. Quaternary glaciation of Muztag Ata and Kongur shan: evidence for glacier response to rapid climate changes throughout the late glacial and Holocene in westernmost Tibet. GSA Bull. 121, 3–4, 348-365.
Seong, Y., Bishop, M., Bush, A., Clendon, P., Copland, P., Copland, L., Finkeel, R., Kamp, U., Owen, L., Shroder, J., 2009b. Landforms and landscape evolution in the skardu, shigar and Braldu valleys, central karakoram. Geomorphology 103, 251–267.
Sharma, P., Bourgeois, M., Elmore, D., Granger, D., Lipschutz, M.E., Ma, X., Miller, T., Mueller, K., Rickey, F., Simms, P., Vogt, S., 2000. PRIME lab AMS performance, upgrades and research applications. Nucl. Instrum. Meth. Phys. Res. B 172, 112–123.
Sharma, S., Chand, P., Bisht, P., Shukla, A.D., Bartarya, S.K., Sundriyal, Y.P., Juyal, N., 2016. Factors responsible for driving the glaciation in the Sarchu plain, eastern zanskar Himalaya, during the late quaternary. J. Quat. Sci. 31, 495–511.
Steck, A., Epard, J., Vannay, J., Hunziker, J., Girard, M., Morard, A., Robyr, M., 1998. Geological transect across the Tso morari and spiti areas- the nappe structures of the Tethys Himalayas. Eclogae Geol. Helv. 91, 103–121.
Taylor, J.R., 1997. An Introduction to Error Analysis, second ed. University Science Books, Sausalito, CA.
Taylor, P., Mitchell, W., 2000. The quaternary glacial history of the zanskar range, north- west indian Himalaya. Quat. Int. 65/66, 81–99.
Thackray, G.D., Owen, L.A., Yi, C., 2008. Timing and nature of late Quaternary mountain glaciation. J. Quat. Sci. 23, 503–508.
Van der Beek, P., Bourbon, P., 2008. A quantification of the glacial imprint on relief development in the French western Alps. Geomorphology 97 (1–2), 52–72.
Zheng, B., Jiao, K., 1991. Quaternary glaciations and periglaciations in the qinghai-Xizang (Tibetan) plateau. In: Excursion Guidebook XI, INQUA 1991, XIII International Congress, Beijing, 54.